NEBRASKA
Good Life. Great Journey.
DEPARTMENT OF TRANSPORTATION

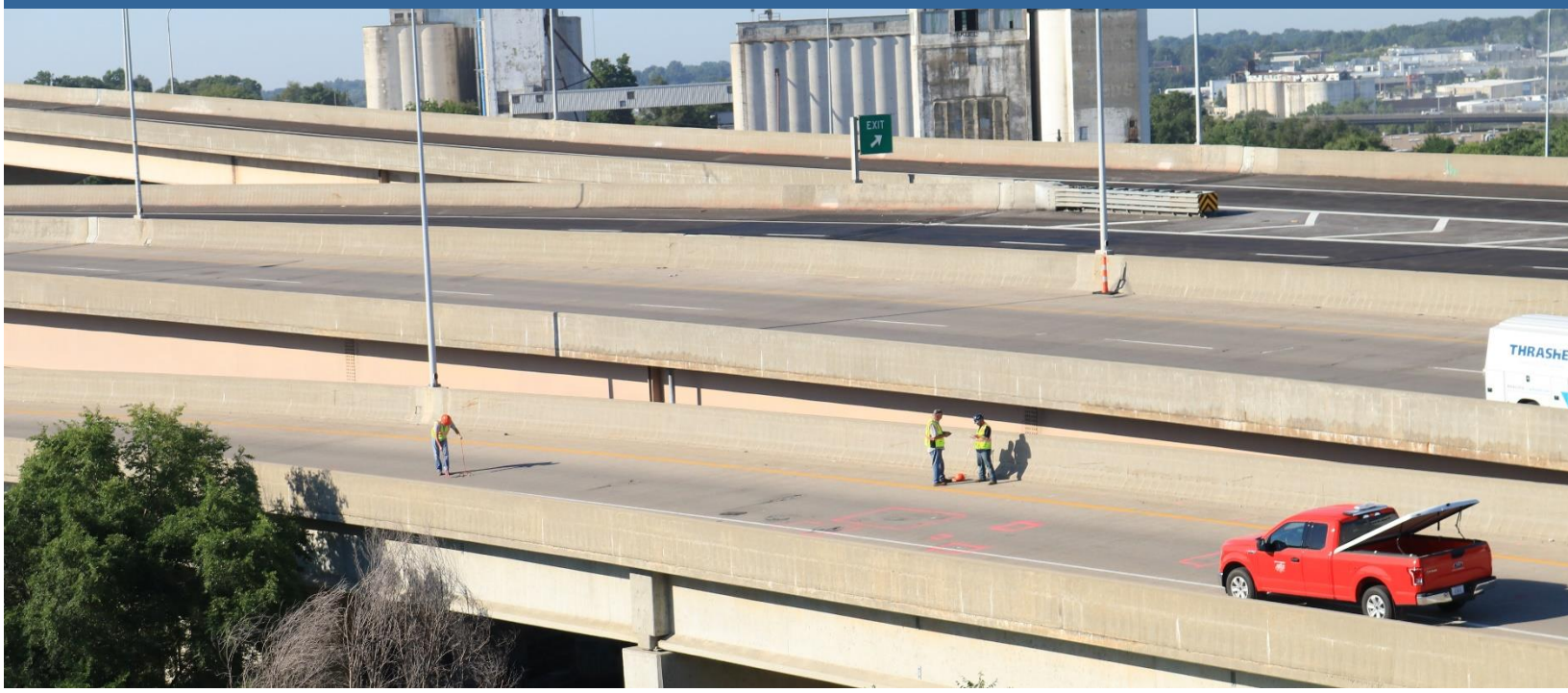

Report SPR-P1(17) M065

Condition Assessment of Bridge Decks with Asphalt Overlay

Sepehr Pashoutani, Jinying Zhu

Department of Civil Engineering
University of Nebraska-Lincoln

December 2019

Technical Report Documentation Page

1. Report No SPR-P1(17) M065	2. Government Accession No.	3. Recipient's Catalog No.	
4. Title and Subtitle Condition Assessment of Bridge Decks with Asphalt Overlay		5. Report Date December 2019	
		6. Performing Organization Code	
7. Author/s Sepehr Pashoutani, Jinying Zhu		8. Performing Organization Report No.	
9. Performing Organization Name and Address Department of Civil and Environmental Engineering. University of Nebraska-Lincoln 1110 S 67th St., Omaha, NE 68182		10. Work Unit No. (TRAIS) 11. Contract or Grant No. SPR-P1(16) M041	
12. Sponsoring Organization Name and Address Nebraska Department of Transportation Research Section 1400 Hwy 2, Lincoln, NE 68509		13. Type of Report and Period Covered July 2016 – December 2019	
		14. Sponsoring Agency Code	
15. Supplementary Notes			
16. Abstract Ground penetrating RADAR (GPR) is a widely used nondestructive testing (NDT) method for bridge deck evaluation. However, the current GPR signal and data processing software and algorithms are not able to provide comprehensive information about bridge deck condition. Although the original objective of this research project was to develop GPR analysis algorithms for condition assessment of bridge decks with asphalt overlay, the scope of work has been expanded to concrete bridge decks with or without overlays. In this study, the research team developed a complete GPR analysis procedure that includes the following components: 1) obtain zero-time for GPR reflection at the deck surface; 2) extract the electromagnetic wave velocity in the cover depth (from surface to top reinforcement mat) using migration method;3) identify rebar positions using automated rebar picking algorithm; 4) extract migrated amplitude at each rebar location; 5) calculate rebar depth using the extracted velocities for all rebars; 6) normalize rebar reflection amplitude and further correct the amplitude using rebar depth. These analyses will provide the following images of bridge deck: surface deterioration condition, cover thickness, velocity in cover concrete (and asphalt overlay), and attenuation. Comparing the amplitude correction methods based on travel time, the proposed depth correction method provides more accurate evaluation of bridge deck deterioration conditions. The developed GPR analysis algorithms have been validated on bridge decks with different types of overlays.			
17. Key Words GPR, bridge deck, overlay	18. Distribution Statement No restriction		
19. Security Classification (of this report) Unclassified	20. Security Classification (of this page) Unclassified	21. No. Of Pages 60	22. Price

Form DOT F 1700.7 (8-72) Reproduction of form and completed page is authorized

Abstract

Ground penetrating RADAR (GPR) is a widely used nondestructive testing (NDT) method for bridge deck evaluation. However, it is still a challenging task for many GPR users to interpret and analyze the large amount of data collected from GPR surveys on bridges. Currently available GPR signal and data processing software and algorithms are not able to provide comprehensive information about bridge deck condition. Although the original objective of this research project was to develop GPR analysis algorithms for condition assessment of bridge decks with asphalt overlay, the scope of work has been expanded to concrete bridge decks with or without overlays.

Most GPR analysis methods use the signal amplitude information only (or attenuation) to evaluate deterioration of concrete bridge decks. In this study, the research team proposed a series of algorithms to extract three types of parameters from GPR signals: direct-coupling wave amplitude on deck surface, wave velocity in cover concrete, and depth-corrected GPR signal amplitude from rebar reflections. Each parameter may reflect defects at different depths of bridge deck, and differentiate surface defects from concrete deterioration and rebar corrosion.

The complete GPR analysis algorithms include the following components: 1) obtain zero-time for GPR reflection at the deck surface; 2) extract the electromagnetic wave velocity in the cover depth (from surface to top reinforcement mat) using migration method; 3) identify rebar positions using automated rebar picking algorithm; 4) extract migrated amplitude at each rebar location; 5) calculate rebar depth using the measured two way travel times and the extracted velocities for all rebars; 6) normalize rebar reflection amplitude and further correct the amplitude using rebar depth. These analyses will provide the following images of bridge deck: surface deterioration condition, cover thickness, velocity in cover concrete (and asphalt overlay), and attenuation. Comparing the amplitude correction methods based on travel time, the proposed depth correction method provides more accurate evaluation of bridge deck deterioration conditions. The developed GPR analysis algorithms have been validated on bridge deck specimens with asphalt overlay.

Disclaimer

The contents of this report reflect the views of the authors who are responsible for the facts and the accuracy of the data presented herein. The contents do not necessarily reflect the official views or policies of the Nebraska Department of Transportation, the Federal Highway Administration, or the University of Nebraska-Lincoln. This report does not constitute a standard, specification, or regulation. Trade or manufacturers' names, which may appear in this report, are cited only because they are considered essential to the objectives of the report. The U.S. government and the State of Nebraska do not endorse products or manufacturers.

Acknowledgments

This research project would not have been possible without the funding provided by the Nebraska Department of Transportation. The authors would also like to acknowledge the engineers at the Department of Transportation for their assistance in this project, and especially Mark Traynowicz, Fouad Jaber, Jason Volz, Kent Miller for providing the bridge information and the arrangements of traffic controls in the field testing.

Contents

List of Figures

List of Tables

Chapter 1

Introduction

Concrete bridge decks constantly undergo physical and chemical degradation with time. Periodic assessment is essential in order to maintain road ways in the loop and provide public safety. Nondestructive evaluation (NDE) or testing (NDT) techniques can provide condition assessment and track deterioration process in bridge decks, and help bridge management agencies make proper maintenance decisions.

Ground Penetrating Radar, also known as GPR, was first introduced in civil engineering as a nondestructive technique in the mid-1990's. GPR transmits electromagnetic (EM) radio waves into the test material and receives echoes from subsurface objects with comparable sizes to the EM wavelength. Advancements in the GPR instruments enable scanning concrete bridge decks in a relatively short time and store the data for further processing. For concrete bridge deck evaluation, the basic principle is to analyze the GPR signal amplitudes from rebar reflections. Concrete deterioration and rebar corrosion will decrease the GPR amplitude and increase the attenuation. In addition, the amplitude can also be affected by the rebar depth and surface condition of bridge deck. Although for some small projects, the radargram formed by B-scan of GPR signals can be directly interpreted by visual inspection, advanced analysis algorithm and software are needed to provide quantitative information about bridge deck deterioration.

GPR signal processing and data analysis methods have been extensively studied for condition evaluation of concrete bridge decks. Common signal processing procedures include: clutter reduction [1], auto-focusing techniques [2, 3], automated rebar picking [4, 5], amplitude-depth correction [6, 7], and velocity analysis [8]. These analysis algorithms result in depth-corrected GPR amplitudes that provide important information about the deterioration condition of concrete bridge decks [6, 9, 10, 7]. Commercial software is also available to analyze GPR signals, such as RADAN [11]. However, these methods

and software still have some limitations in practice. These limitations include lack of consistency in amplitude measurement, no EM wave velocity information in concrete, rebar depth variation, effect of bridge deck surface condition on amplitude, etc.

Research presented in this report will address the current knowledge gaps, clarify some common confusions, and provide a complete GPR signal analysis procedure for bridge deck evaluation. These developed analysis algorithms are first applied to simulated GPR signals to improve understanding of the GPR principles. Then the procedure is implemented on real bridge GPR data and the results are presented in the forms of 2D images of surface reflection, velocity, cover thickness, and attenuation of the bridge deck.

1.1 GPR background

GPR uses short-duration high-frequency (0.1 ~ 2.6 GHz) EM wave pulses to image sub-surface. The EM wave travels at the speed of light (c = 30 cm/ns [11.8 in/ns]) in the vacuum while its velocity in a medium is a function of the medium's dielectric permittivity. Permittivity ϵ is a complex parameter with the imaginary part representing loss. In practice, the real component is usually presented as the relative permittivity ϵ_r which is normalized by ϵ_0 of the free space. The wave velocity in a medium v_m can be determined from Eq. 1.1.

$$v_m = \frac{c}{\sqrt{\epsilon_r}} \tag{1.1}$$

For an object embedded in the medium at a distance d, the required time t for the EM wave to reach and reflect back from the object is called two-way travel time (TWTT), which is calculated as $t = 2d/v_m$.

Figure 1.1 shows a schematic diagram of the GPR antenna sending a plane EM wave and receiving reflections from a rebar embedded in concrete. Symbols A_1 to A_4 represent the amplitudes of the plane wave at the end of each travel path. The corresponding wave paths are

- A_0: the source signal generated by the GPR system;
- A_1 and A_2: the direct signals between the transmitter and receiver, through air and concrete surface respectively;
- A_3: the penetrating wave in concrete cover before rebar reflection;
- A_4: the received signal by the antenna from rebar reflection.

Reflection and transmission occur at an interface of two media with different permittivity values. The reflection (R_{12}) and transmission (T_{12}) coefficients of an EM wave entering from

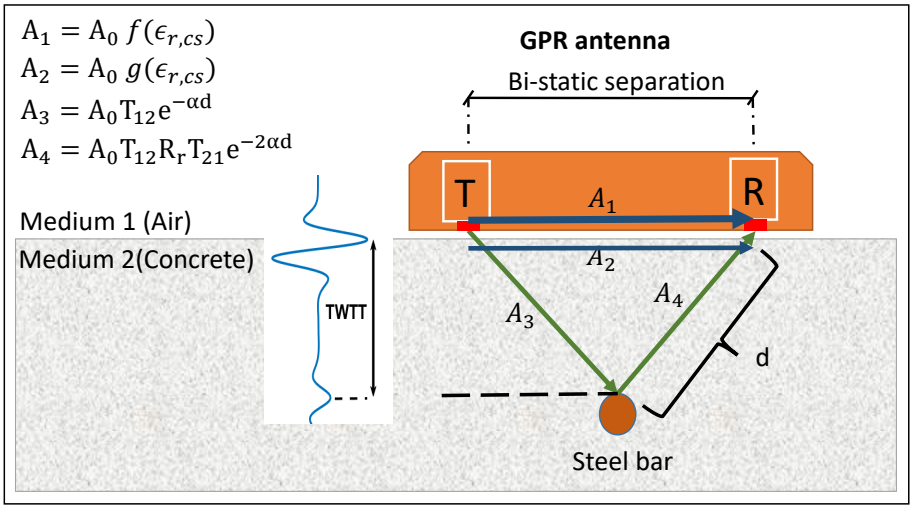

Fig. 1.1. Schematic diagram of GPR antenna and EM wave propagation in concrete with an embedded rebar.

material 1 to 2 follows Eqs. (1.2) and (1.3), where ϵ_{r1} and ϵ_{r2} are the relative permittivities of the first and second media respectively. Coefficients T_{12} and T_{21} represent the transmission coefficients of EM wave transmitting from the medium 1 to 2 and vice versa. R_r is the reflection coefficient from the rebar and α represents the absorption coefficient of the second medium. R_r may be affected by the surface and corrosion condition of rebars.

$$R_{12} = \frac{\sqrt{\epsilon_{r1}} - \sqrt{\epsilon_{r2}}}{\sqrt{\epsilon_{r1}} + \sqrt{\epsilon_{r2}}} \tag{1.2}$$

$$T_{12} = 1 + R_{12} \tag{1.3}$$

$$\epsilon_{r,cs} = \left(\frac{1 + A_s/A_p}{1 - A_s/A_p} \right)^2 \tag{1.4}$$

Figure 1.2 shows a typical GPR B-scan recorded on a concrete bridge deck. The high amplitude strip occurred before 2 ns indicates the antenna coupling with the concrete surface (mixed signals of A_0 and A_1). The hyperbolas marked with yellow rectangles show the reflections from two rebars. Hyperbolas with strong reflection amplitude generally represent sound concrete and rebars where the absorption coefficients are small and the reflection coefficient R_r is close to 1. On the other hand, when concrete deteriorates and steel reinforcements corrodes overtime, the conductivity and attenuation coefficient α of

concrete increase, and the reflection coefficient of steel drops. The hyperbola with weak reflection is indicative of concrete deterioration and/or rebar's corrosion.

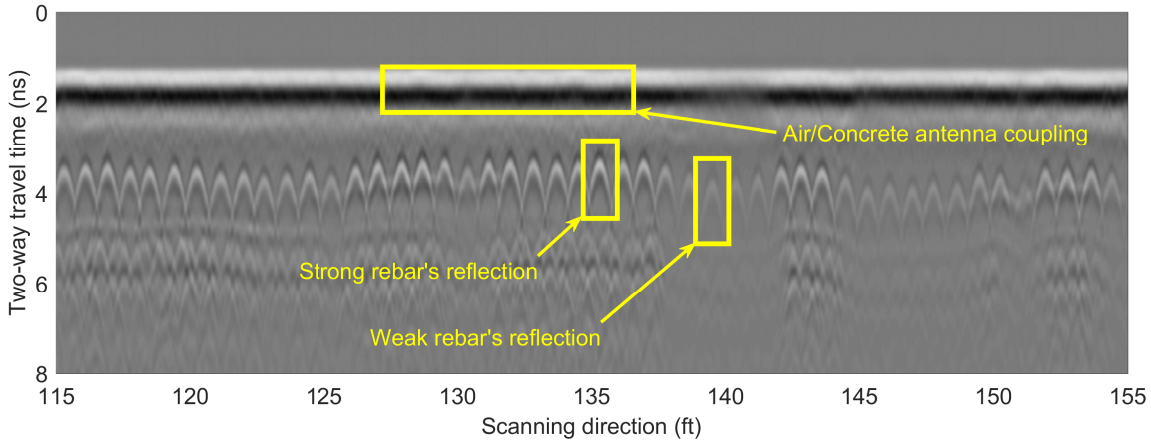

Fig. 1.2. Typical GPR B-scan image from a concrete bridge deck.

1.2 GPR system description

A Ground Penetrating Radar system generally consists of a control computer and an antenna. The computer provides power to the antenna, set measurement parameters, and stores recorded data. The antenna box contains a transmitter module to send electromagnetic pulse and a receiver to receive echoes from surface and subsurface interfaces. Depending on the surface coupling condition, GPR antennas can be classified as air-coupled and ground-coupled. Air-coupled antenna are used for fast scanning and preliminary deterioration investigations. They can be mounted on a vehicle and scan pavements or bridge decks at the traffic speed. Because of high test speed, the air-launched GPR typically has a lower spatial resolution than ground-coupled GPR, and it is often used for quick scanning to provide rough estimates of the surface and subsurface deterioration condition. For detailed and in-depth survey, ground-coupled antenna is preferred. A survey cart, shown in the Figure 1.3, is usually used for ground-coupled GPR survey at a walking speed, therefore traffic control is needed. In this report, research team used ground-coupled antennas for detailed scanning and data analysis.

The center frequency of the antenna determines the maximum penetration depth of EM wave and the vertical resolution of the B-scan image. Increasing the frequency will improve the image resolution at the cost of decreasing the penetration depth. In most bridge deck

inspections with ground-coupled antennas, EM wave with a center frequency of 1.5 GHz provides sufficient penetration depth and adequate resolution. The time range determines the total time that GPR records the reflections from the subsurface. The proper time range can be determined by the expected penetration depth and velocity information.

Fig. 1.3. GPR equipment at UNL NDT laboratory

In this project, two GPR systems GSSI SIR-3000 and SIR-4000 with scanning carts were used to scan the bridges in the field testings. The SIR-4000 system provides data with better signal resolution and higher acquisition rate than the SIR-3000 system. The survey cart is equipped with a wheel encoder to record the travel distance along each scan line. In addition, a Real Time Kinematic (RTK) GPS connected to a laptop or tablet computer was added to the scanning cart to record the real time locations of GPR scans on bridges.

1.3 Research objectives and knowledge gaps

The original objective of this work was to evaluate the performance of NDT methods in condition assessment of concrete bridge decks with asphalt overlay. During the literature review, the authors realized there are many limitations in the current GPR data processing

methods, and decide to expand the scope of work to develop and improve GPR signal processing algorithm for all types of concrete bridge decks with or without overlays.

The limitations in the current GPR analysis methods are listed as follows:

- **Rebar positions.** In order to extract the amplitude of rebar reflections, rebars should first be identified so that their positions and depth are determined. Currently, the commercial software RADAN (GSSI) [11] needs manual interaction for rebar picking, which is time consuming for large data sets. Although some automated rebar picking algorithms are developed based on pattern recognition, curve fitting [12] or migration [13], these methods need complex machine learning algorithms to reduce false rebar picking.
- **Amplitude.** Rebar reflections are shown as hyperbolas in GPR B-scan images. The authors often found that the amplitude picked at the apex of the hyperbola may not be the maximum amplitude, neither represent the condition of concrete and rebar. It is better to focus the energy distributed in the hyperbola into a small region using the migration algorithm. The migrated amplitude is more robust and consistent than the raw signal amplitude picked from the hyperbola.
- **Zero time offset.** Zero time is the arrival time of GPR signal reflection from the bridge deck surface. Accurate zero time and EM wave velocity in concrete are needed in order to perform migration algorithm properly. There is still no clear criterion for zero-time determination.
- **Velocity and rebar depth.** In real bridge decks, the velocity is not constant but varies with the condition of concrete. Most current GPR analysis methods assume a constant velocity value for the entire bridge deck, which will cause errors in the migrated amplitude. In addition, with an assumed constant velocity, the rebar depth cannot be accurately determined.
- **Surface condition.** Most of the current GPR analysis methods neglect the effect of bridge deck surface condition which actually greatly influences the amplitude of rebar reflection. The rebar reflection amplitude is affected by the air-concrete interface, where a portion of energy is reflected back to air/antenna, and only the transmitted portion reaches rebars. The surface reflection is governed by the relative permittivity of the concrete surface. Extracting the surface reflection signals not only helps correct the effect of surface condition on rebar reflection, but also provide information about the concrete surface condition.
- **Depth-correction.** EM wave traveling in a dielectric medium (concrete) dissipates with distance. Therefore, reflections from deep objects in the medium has lower

amplitude than shallow objects. Since in a concrete bridge deck cover thickness over all rebars is not constant, change of amplitude due to variation of cover thickness should be addressed. The common practice is to adjust the amplitude of rebar proportionate to its TWTT. But rebars in concrete with low wave velocity have high TWTT and this procedure will provide inaccurate amplitudes.

In this study, the authors addressed the above mentioned challenges and proposed corresponding solutions. A complete GPR analysis algorithm is developed to automate the GPR signal analysis and rebar picking. Multiple GPR parameters will be used to map/image the tested bridge deck and identify defects and deterioration regions. The complete GPR analysis procedures include the following steps:

1. Obtain zero-time for GPR reflection at the deck surface;
2. Extract the electromagnetic wave velocity in the cover depth (from surface to rebar top) using migration method;
3. Identify rebar positions using automated rebar picking algorithm;
4. Extract migrated amplitude at each rebar location;
5. Calculate rebar depth using the two way travel times and velocities for all rebars;
6. Normalize rebar reflection amplitude by the surface condition; and
7. Correct the amplitude with rebar depth.

1.4 Report overview

This report presents the findings of the research conducted in the Nondestructive Testing Laboratory of Department of Civil Engineering at the University of Nebraska-Lincoln in collaboration with the Nebraska Department of Transportation (NDOT). **Chapter** 1 presents introduction of GPR principles and system description, and summarizes the research objectives and current gaps in the GPR data processing. **Chapter** 2 presents the detailed GPR signal processing procedures step by step. In this chapter, the above mentioned challenges are addressed and solutions are proposed to improve GPR analysis for concrete bridge deck evaluation. In **chapter** 3, the developed GPR data processing algorithms are implemented on the GPR data collected from three bridges in Nebraska, and the results are compared with old methods. In **chapter** 4 key findings from this project are presented and discussed. The authors also propose future work to be studied for further improvement of GPR analysis.

Chapter 2

GPR signal processing algorithms and procedures

In order to get better understanding of GPR wave propagation in reinforced concrete, numerical simulations were performed using an open source software gprMax [14]. This software simulates EM wave propagation using the Finite-Difference Time-Domain (FDTD) method for numerical modelling of GPR [14]. Figure 2.1(a) shows the geometry of a 2D model for gprMax simulation. The model simulates two concrete blocks, arranged side by side, with the relative permittivity of $\epsilon_r = 5$ for the left block and $\epsilon_r = 10$ for the right one. In each block, a cylindrical object (diameter 16 mm) of perfect electric conductor (PEC) material is embedded to simulate steel reinforcements. The concrete cover over the reinforcements are 9.2 cm.

A steel plate is defined on the top left corner of the concrete block for measuring the EM wave reflection amplitude from a PEC material on the surface. Since the reflection coefficient of the steel plate is close to 1 and it reflects all energy, objects under the steel plate cannot be identified.

A ground-coupled antenna is usually enclosed in a protective box which is not in direct contact with concrete. In this simulation, the antenna is elevated 1.6 cm from the ground surface. The center frequency of the antenna is 1.5 GHz, which is commonly used for bridge deck scan. The transmitter and the receiver are 2 cm apart. Figure 2.1(b) shows the B-scan image of the model from gprMax simulation.

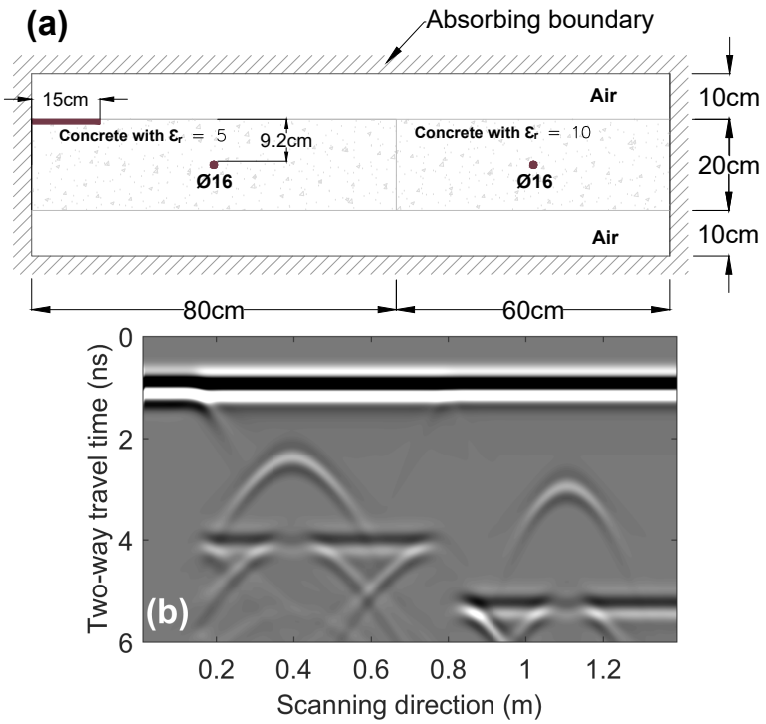

Fig. 2.1. (a) Model for gprMax simulation, (b) GPR B-scan image of the gprMax model.

2.1 Surface reflection

For a ground-coupled antenna placed very close to the concrete surface, the reflected waves from the surface and subsurface are mixed with direct waves through air and concrete from the transmitter to the receiver. The high amplitude of direct air wave not only masks reflections from the concrete surface and near surface rebars, it also makes it difficult to determine the true zero time from surface reflection. According to studies by [15] and [16] the early GPR signal attributes (direct coupling wave) are sensitive to the permittivity and conductivity of the medium when a ground-coupled antenna is used. Both studies show that as the permittivity of the material increases, the direct coupling wave amplitude decreases exponentially. In the ranges of concrete permittivity $\epsilon_{rc} = 4 \sim 13$ the amplitude is sensitive to change of permittivity.

The authors also investigated the effect of near surface permittivity of concrete on the direct coupling wave amplitude. A GSSI SIR-4000 system was used to scan a specimen that was cut from a bridge deck before demolition, as shown in the Figure 2.2(a). GPR signals were collected in two steps with different liftoff heights. First the GPR antenna (1.5 GHz) was placed at a height of 25 cm from the concrete surface where the reflecting signal from

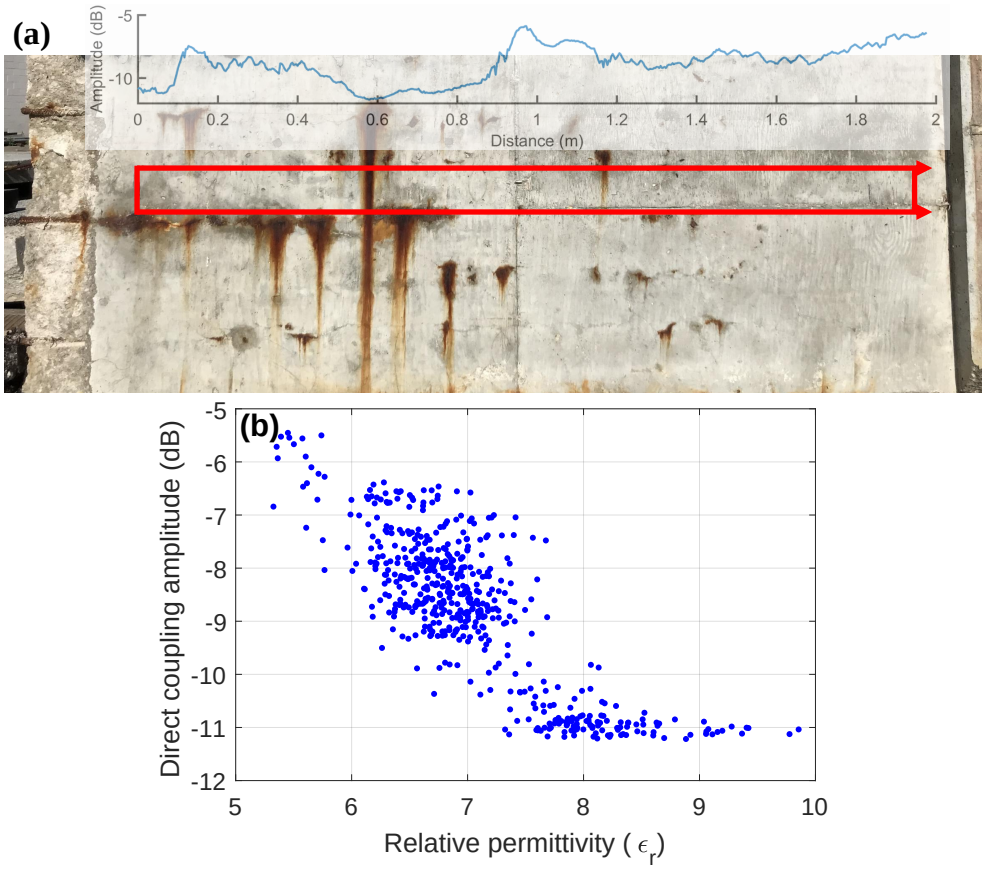

Fig. 2.2. Direct coupling amplitude versus relative permittivity of the concrete specimen

concrete is distinguishable from the direct air wave. In this setup, the permittivity of the concrete surface can be calculated using Eq. (1.2). Then the antenna was placed close to the surface and the GPR data were collected on the same path as in the first step. Figure 2.2(b) then plots the direct coupling wave amplitude vs. the permittivity calculated in step one. The result of this test suggests that permittivity of the concrete surface is correlated to the direct coupling wave amplitude recorded by the GPR with a ground-coupled antenna. Therefore, instead of using permittivity of concrete surface, the direct coupling wave amplitude can be used for evaluation of concrete surface conditions. In Figure 2.2(a), the direct coupling wave amplitudes were also plotted on the specimen surface to visually confirm that the amplitude of the GPR data matches the surface condition variation. The results of this test agree with the theoretical and experimental results found in literature [15, 16].

2.2 Zero time and TWTT

For a ground-coupled GPR scan, the time zero t_0 is regarded as the arrival time of surface reflection. Accurate time zero is important in GPR signal analysis in order to determine the depth of objects and EM wave velocity in concrete. Yelf [17] compared multiple methods used in practice and proposed 0.61 ns prior to the first positive peak as the zero time t_0 for a 1.5 GHz bow-tie antenna. This method was also used by Dinh et al. [4, 18] for bridge deck evaluation. In this paper, the authors attempt to determine the zero time t_0 and TWTT from surface reflection wave after direct air wave subtraction.

In order to obtain accurate EM wave arrival time of the surface reflection, the authors propose a method of subtracting the direct air wave from all traces. In practice, the direct air wave can be measured at the time of GPR survey by pointing the antenna toward an open space without reflective objects, then record and average enough number of A-scans to reduce effect of random noise. This is necessary especially if different antennas or systems with other data file types (8 bit, 16 bit, or 32 bit) have been used for data collection.

Figure 2.3 shows simulated signals from the the gprMax model presented in Figure 2.1(a), when the antenna is elevated 1.6 cm above the surface. Figure 2.3(a) shows the raw GPR A-scan signal over the left steel rebar, and Figure 2.3(b) presents the signal after the direct air wave is subtracted. Figure 2.3(c) shows the B-scan image on the model after direct air wave subtraction. In theory, both reflections at the air-concrete and concrete-steel interfaces should have the same phase, as predicted by Eq. (1.2). However, due to direct air wave interference, the first two reflections in Figure 2.3(a) have opposite phases. After direct air wave subtraction, the air-concrete and the concrete-steel reflections in Figure 2.3(b) have the same phase. Therefore, the TWTT for the EM wave travelling between the concrete surface and the top of rebar can be obtained from the time difference between the positive peaks $t_r - t_s$, (see Figure 2.3(b)). In Figure 2.3(b), TWTT from the concrete surface and the top of rebar is calculated from two positive peaks, which is $t_r - t_s = 1.387$ ns. Compared to the expected TWTT 1.372 ns in concrete ($\epsilon_r = 5$), the TWTT determined by this method has an error of 1.1%, which is more accurate than TWTT determined from the raw signal.

In the gprMax simulated signal, the zero time t_0 is the first break point on the surface reflection. In order to check if this method can be applied to real signals, Figure 2.4 presents a measured GPR signal using a GSSI 1.5 GHz ground-coupled antenna at 12 mm above the concrete surface. The direct coupling wave and the signal after direct air wave subtraction are also shown. The break point on the surface reflection occurs at 1.26 ns. According to Yelf [17], the zero time occurs at 0.61 ns prior to the first positive peak on the raw signal.

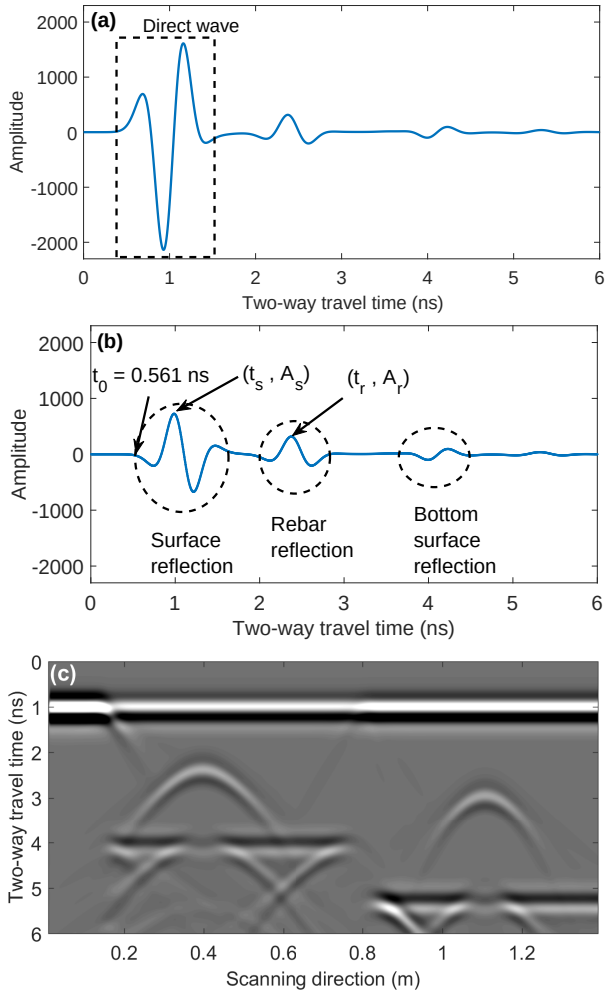

Fig. 2.3. (a) A-scan over the left rebar mixed with the direct air wave, (b) A-scan over the left rebar when the direct air wave is subtracted, and (c) B-scan image after the direct air wave is subtracted from all traces.

It should be noted that a different antenna was used in [17], and the signal in [17] had an opposite phase from the signal obtained with the GSSI GPR system. Therefore, the arrival time t_0 should be taken at 0.61 ns prior to the first negative peak when using the method by Yelf. The first negative peak of the raw signal occurs at 1.875 ns, and 0.61 ns prior to it gives 1.265 ns as t_0, which agrees very well with the method proposed in this study.

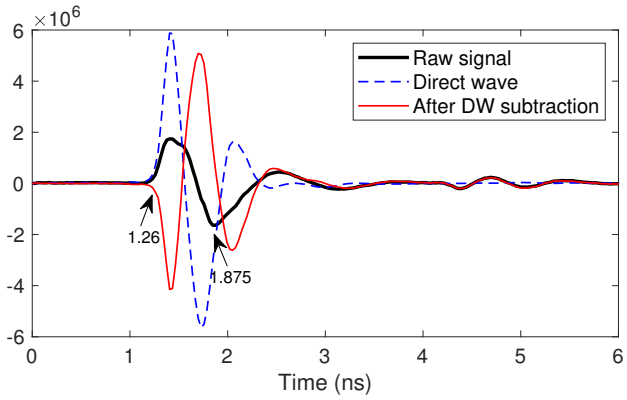

Fig. 2.4. GPR signal measured with a GSSI 1.5 GHz antenna at 12 mm above concrete surface.

2.3 Clutter reduction

In a GPR B-scan image, the strong direct air wave and surface reflections obscure weak reflections from deep objects. Reflections from other subsurface scatterers and above ground objects may also introduce disturbance. Several clutter reduction algorithms have been previously studied in [1, 19] to remove these effects. Mean subtraction method is the simplest algorithm which targets the repetitive properties of the clutter in the B-scan. In Eq. (2.1), A_{ms} is the data after mean subtraction

$$\mathbf{A}_{ms}(i,j) = \mathbf{A}(i,j) - \frac{1}{n}\sum_{j=1}^{n}\mathbf{A}(i,j) \tag{2.1}$$

where $\mathbf{A}(i,j)$ denotes the raw signal amplitude at i^{th} sample in the j^{th} trace, and n is the number of traces. The main disadvantage of the mean subtraction method is that it influences both the clutter and objects' reflection in the medium. The performance of this method decreases when there is a significant variation in concrete bridge deck surface condition along the scanning direction. In this work, the mean subtraction method is only

implemented on a small segment of B-scan each time to avoid artifacts. The output of this method on the simulated model is discussed in the auto-focusing section.

2.4 Auto-focusing

Round shaped dielectric interfaces appear as hyperbolas in the GPR B-scan. The signal amplitude along each hyperbola depends on the surface condition, medium spatial electrical properties, and the shape of the object. In practice, it has been observed that the peak reflection amplitude of a rebar is not always on the vertex of the hyperbola. In order to obtain accurate reflection amplitude and the position of the object, migration algorithm can be used to transform the unfocused space-time hyperbolic signature to a few image pixels at the true rebar location. Migrated amplitudes are used in all analyses presented in this study.

Ozdemir et al. [3] has reviewed various migration algorithms and evaluated their performance. The frequency-wave number (f-k) migration method [20] is used in this study due to its fast computation time. The migration techniques require the actual zero time and the true EM wave velocity in media. When the correct parameters are used, these methods can successfully reconstruct the B-scan image so that all reflected energy from a rebar focuses to a few image pixels. For migration of rebar reflections, the zero time of a B-scan image should be set at t_0, which is the first arrival time of concrete surface reflection (see Figure 2.3(b)). This procedure is called zero offset.

In real concrete structures, the EM wave velocity profile in concrete along the scanning direction is not constant, which depends on the concrete conditions. According to Eq. (1.1), the EM wave velocity is a function of the relative permittivity of the medium. When the bridge deck cracks, or deicing salt and chloride seeps into the concrete, constant velocity migration will not give accurate results. Figure 2.5 show the reconstructed image when a constant velocity profile was used for the entire B-scan image. In Figure 2.5(a), $\epsilon_r = 5$, the left rebar is properly focused, but the right rebar is over-migrated (upward); in Figure 2.5(b), $\epsilon_r = 7.5$, the left bar is under-migrated (downward), while the right one is over-migrated; in Figure 2.5(c), $\epsilon_r = 10$, the right rebar is properly focused. Therefore, a constant wave velocity will not be able to focus all rebars in a large B-scan image.

Several practical image-based metrics have been implemented and evaluated by Wei and Zhang [2] to measure the performance of migration through an automated process in order to eliminate human decision. A GPR B-scan with m samples and n traces in the time-domain is represented as a matrix of amplitudes, with μ and σ representing the mean and standard deviation of the elements of the matrix respectively. Among all the metrics

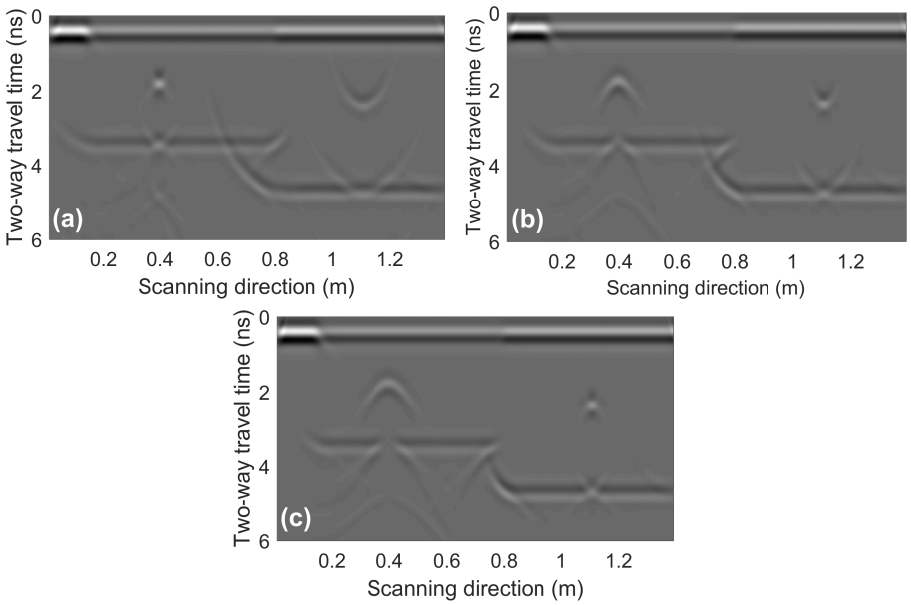

Fig. 2.5. Migration using a) $\epsilon_{rc} = 5$, b) $\epsilon_{rc} = 7.5$, and c) $\epsilon_{rc} = 10$.

investigated in [2], the High-Order Statistics [21] is the most sensitive one to the change of wave velocity and less affected by the signal to noise ratio variation. The metrics is given by Eq. (2.2)

$$H(k) = \frac{\sum_{i=1}^{m} \sum_{j=1}^{n} (|\mathbf{A}'_{ms}(i,j)| - \mu)^k}{(mn-1)\sigma^k}, \tag{2.2}$$

where $\mathbf{A}'_{ms}$ represents the matrix after migration and mean subtraction. The sensitivity of the metric to wave velocity change is a function of its order k.

In order to determine the true velocity, migration is performed for a range of possible velocity values (or relative permittivity values ϵ_{rc}) in concrete. The metric H is then calculated for each matrix after migration $\mathbf{A}'_{ms}$. According to [2], when the correct wave velocity is used to reconstruct the matrix $\mathbf{A}'_{ms}$, the metric $H(k)$ reaches the maximum value. They found for $k = 10$, the metric $H(10)$ has high sensitivity to velocity change and good performance even for GPR data with low signal to noise ratios. Using this metric requires splitting the large matrix $\mathbf{A}$ into sub-matrices containing at least one hyperbola. As an example, the matrix $\mathbf{A}$ from the simulated gprMax model (Figure 2.3(c)) was split into two sub-matrices shown in the Figure 2.6(a). Figure 2.6(b) presents images of the two sub-matrices after clutter removal using Eq. (2.1). In Figure 2.6(c), the metric $H(10)$ clearly indicates the correct relative permittivity for both sub-matrices. Figure 2.6(d) shows the

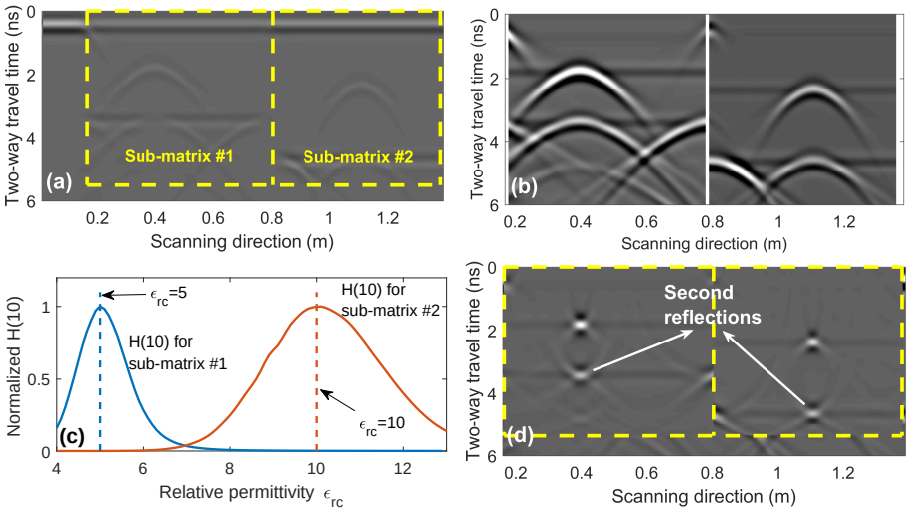

Fig. 2.6. a) Extracted sub-matrices, b) sub-matrices after clutter removal, c) H(10) for sub-matrices in a range of $\epsilon_{rc} = 4 \sim 13$, d) reconstructed B-scan using migration.

final stage of the migration process where correct velocity values were used for the B-scan image reconstruction.

In cases of real bridge data, a B-scan matrix can be separated into many sub-matrices containing one or more hyperbolas, and the average velocity of each extracted block of data can be estimated using this metric $H(10)$.

2.5 Automated rebar reflection picking

When GPR is used for concrete bridge deck evaluation, rebar positions should be first located on B-scan images, and then the amplitudes of rebar reflections are used to detect deterioration of bridge decks. In a typical GPR bridge survey, manually locating rebars and measuring their corresponding amplitudes is time-consuming. In Figure 2.6(d), it is noticed that the migrated image has the highest amplitudes at the rebar location, which are identified easily. We developed a MATLAB function, *AutoPick*, to identify the focused rebar locations on a migrated B-scan image, which was briefly discussed in [22]. This function is based on an assumption that there must be one rebar in every specified spacing S, where the focused rebar reflection has the most significant amplitude compared to other traces. After removing the clutter and reconstructing (migration) the image using the correct wave velocity profile, the strongest reflections in the concrete B-scan image are caused by rebars in the concrete. These peaks with regular spacing can be easily detected by a peak

detection algorithm. It has been shown that the algorithm is simple and efficient with high success rate, and needs minimum human interaction in the process.

Figure 2.7(a) presents one raw B-scan from a real bridge GPR survey. The rebar positions from the *AutoPick* function is shown in Figure 2.7(b) with the zoomed view in Figure 2.7(c). There are 559 rebars in this B-scan, and all rebars are correctly identified. The entire GPR survey on the bridge has 13 scans, and 7235 rebars. The developed *AutoPick* procedure missed 14, and falsely picked 20 rebars. The overall accuracy rate is 99.5%.

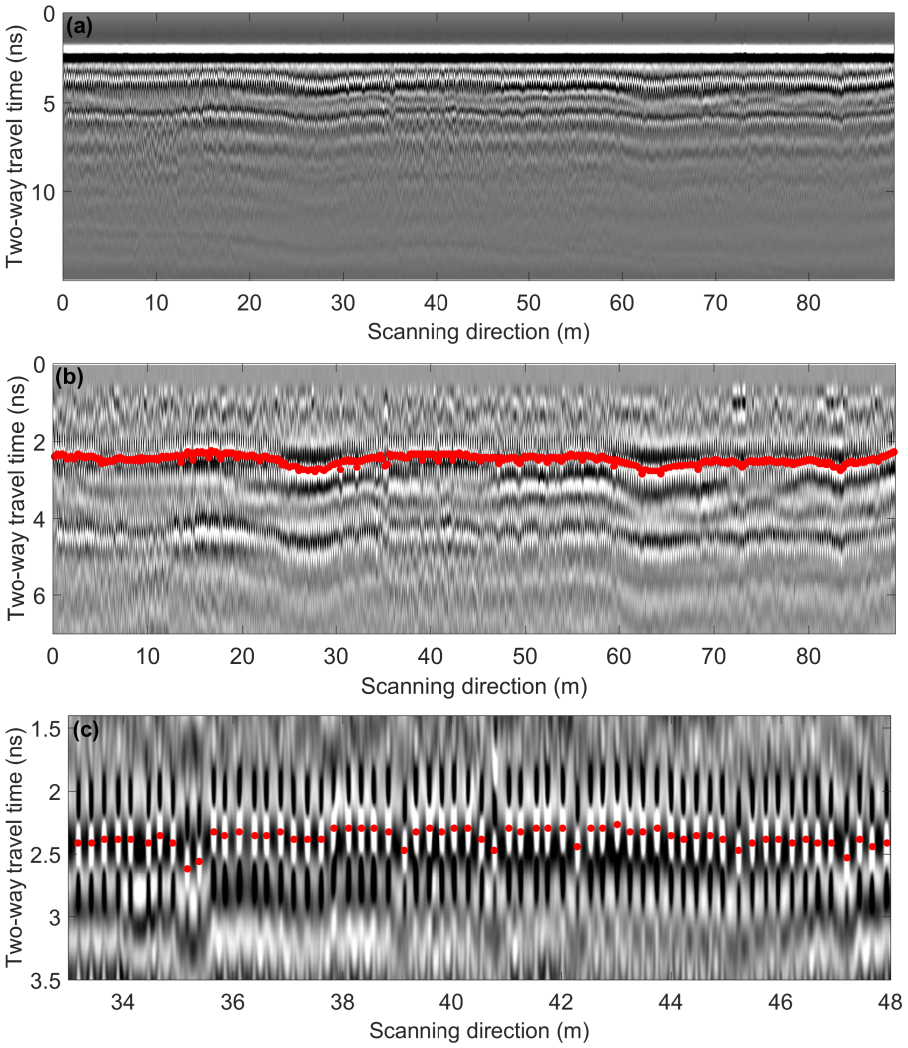

Fig. 2.7. Automated rebar picking demonstration. (a) A raw B-scan image, (b) *AutoPick* output, and (c) zoomed view of the detected rebars from 33 to 48 m.

2.6 Normalization of rebar amplitude

For concrete in good condition with low moisture content, the relative permittivity of concrete will be in the range of $\epsilon_r = 5 \sim 6$. On the other hand, a larger relative permittivity indicates high concrete porosity, existence of moisture and chloride. According to Eq. (1.2), the reflection coefficient (R) at the air-concrete interface increases with the relative permittivity of concrete surface, which indicates that less energy penetrates into concrete. Therefore, the amplitude of rebar reflection is affected by near surface concrete conditions.

The rebar reflection amplitude is affected by the transmission coefficients at the air/concrete interface (T_{12} and T_{21}), rebar condition R_r, and attenuation in concrete $e^{-\alpha d}$, which can be seen from Figure 1.1. Determining the T_{12} and T_{21} are rather complicated. In the previous section (2.1 Surface reflection), the direct coupling wave amplitude is shown to decrease with the permittivity of the concrete surface. High permittivity also causes low transmission of the EM wave. Therefore, the authors propose to normalize each rebar's reflection amplitude with the direct coupling wave amplitude (A_{dc}) measured directly above the rebar,

$$A_{norm} = 20 \log(\frac{A_4}{A_{dc}}). \tag{2.3}$$

After normalization, the amplitude A_{norm} depends on R_r and $e^{-\alpha d}$ only. Therefore, the normalized amplitude represents the combined condition of rebar corrosion and concrete internal deterioration.

The proposed normalization is different from what suggested by GSSI manual [11], where the amplitudes of rebar reflections are normalized by a constant number, which is $2^{15} - 1$ for 16 bit data, and $2^{31} - 1$ for 32 bit data. Some researchers [7] use the average amplitude of direct-coupling waves from the entire bridge scans to normalize rebar reflections, which is equivalent to normalization with a constant number, and does not address surface condition variations.

A GPR B-scan from a bridge deck with visible surface deterioration (Figure 2.8(a)) has been investigated for two normalization methods. The green rectangles highlight regions of the deck with weak direct coupling wave and weak rebar reflections, which indicate high surface dielectric permittivity. Scatter plots are used to correlate the rebar reflection amplitude vs. TWTT as in references [6, 7], where the TWTT was calculated from the signal after direct air wave subtraction. For comparison, rebar reflection amplitudes using the two normalization techniques are presented in Figures 2.8(b-c). In Figure 2.8(b), the rebar reflection amplitudes are normalized by the first positive peak amplitude of the direct air wave (a constant number). Figure 2.8(c) plots the rebar amplitudes normalized by the

direct coupling-coupling amplitude above each rebar. Since the direct air wave has a higher amplitude, the normalized data in Figure 2.8(b) has lower amplitudes than in Figure 2.8(c).

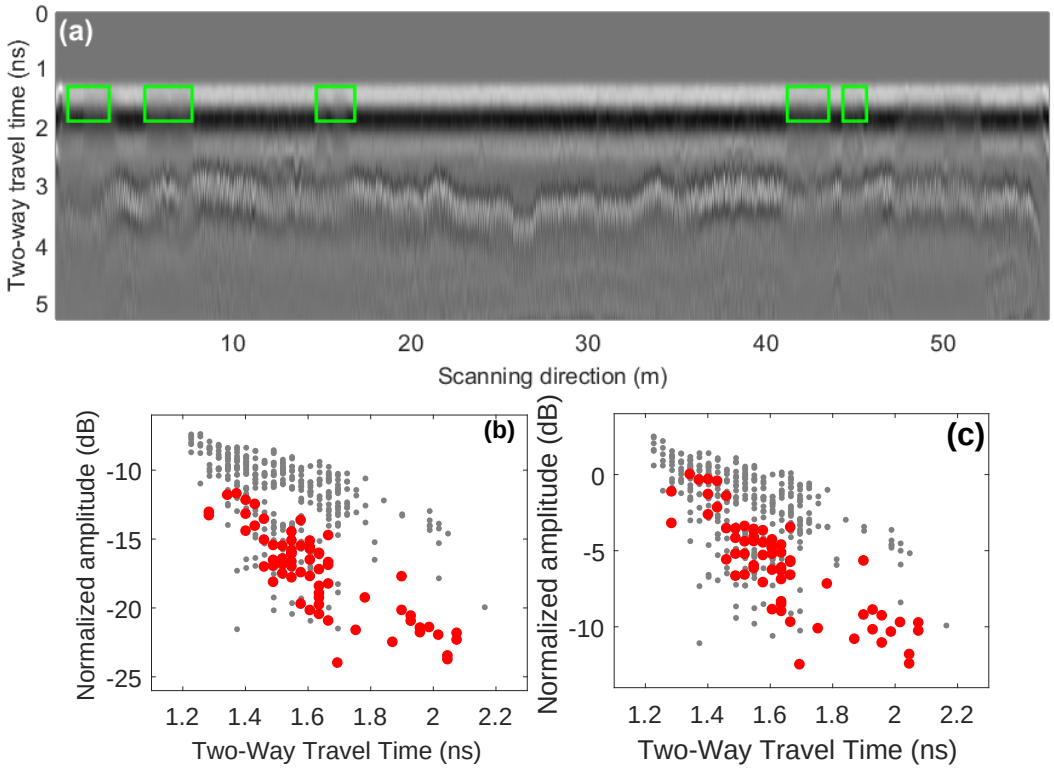

Fig. 2.8. (a) GPR B-scan collected from a bridge deck; scatter plots of rebar amplitude vs. TWTT normalized by (b) the direct air wave, (c) the mixed surface reflection.

In order to visualize the differences between two normalization methods, the data points directly under the highlighted locations on the B-scan Figure 2.8(a) are shown in red color in Figure 2.8(b) and 2.8(c). In Figure 2.8(c), these highlighted points move up relative to the other data points when normalized by the proposed method. This result indicates that the original low amplitudes of these points were partially caused by bad surface conditions. With the proposed normalization method, it is possible to differentiate the surface anomalies from the concrete cover deterioration and rebar corrosion.

2.7 Depth correction of rebar amplitude

In practice, it is common for rebars to deviate from their designated positions and thus the cover thickness varies in a bridge deck. These variations have to be addressed in GPR

analysis in order to reduce the effect of EM wave geometric and dielectric loss on rebars reflection amplitudes [7]. Then the rebar reflection amplitudes measured at different depths can be compared, and a final deterioration map can be plotted.

Rebar depth information in most cases is not available in practice. The commonly used depth correction method is to establish the 90^{th} percentile linear regression relationship between rebar reflection amplitudes against their TWTT, either using the collected data from the test bridge [6], or using the relationship from a reference bridge or sound regions of a bridge deck [7, 22]. This relationship is then used as a reference to correct rebar reflection amplitudes for rebar depth variation.

Since the purpose of depth correction is to reduce the effect of geometric spreading and dielectric loss of EM waves in concrete, the proper depth correction should be based on amplitude vs. rebar depth relationship. In this study, the actual rebar depth can be calculated using the measured TWTT and the extracted wave velocity information for each rebar. Therefore, the amplitude can be corrected with the actual rebar depth instead of TWTT.

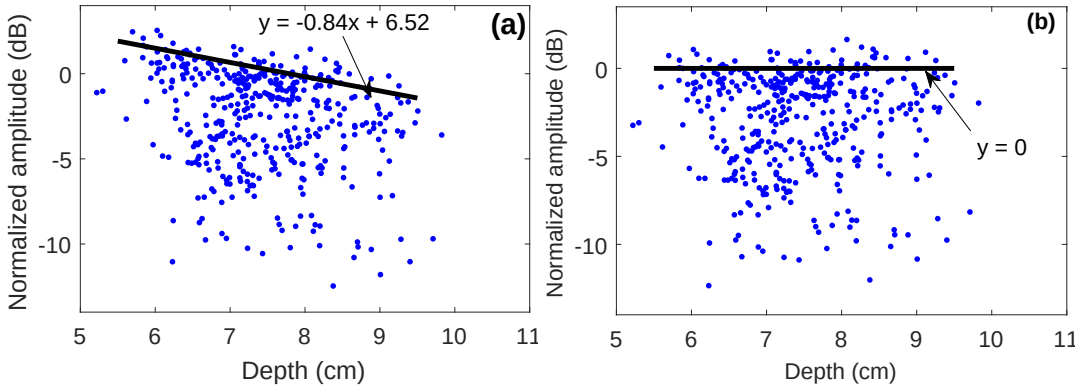

Fig. 2.9. Scatter plots of rebar reflection amplitude versus depth, (a) before depth-correction, and (b) after depth-correction.

The slope of the 90^{th} percentile regression line of these data points indicates the rate of amplitude loss due to geometric spreading and dielectric loss with depth. Figure 2.9(a) shows the scatter plot of the normalized rebar reflection amplitude vs. rebar depth for the GPR B-scan shown in Figure 2.8(a), and the 90^{th} percentile linear regression line is given. The slope of the regression line represents the rate of EM wave attenuation with depth in concrete. This value may vary depending on concrete property and overlays. Figure 2.9(b) shows data points after depth correction, by subtracting the regression equation shown in Figure 2.9(a). After depth correction, data along the 90 percentile line have an amplitude

of zero dB, which indicates that all other data points are further normalized by these data for each rebar depth. Therefore the depth corrected amplitude will have 10% data points with amplitude above zero dB. In Figure 2.9(b), most data points concentrate in the range of [-6,0] dB. A threshold value may be determined from visual inspection of the scatter plot of statistical analysis.

2.8 Cover depth determination

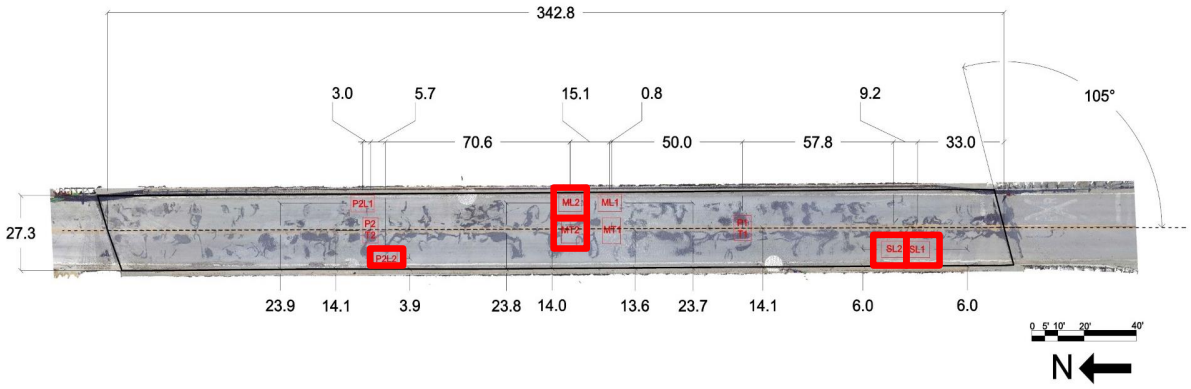

Fig. 2.10. Location of the specimens on the Big Nehama river bridge deck

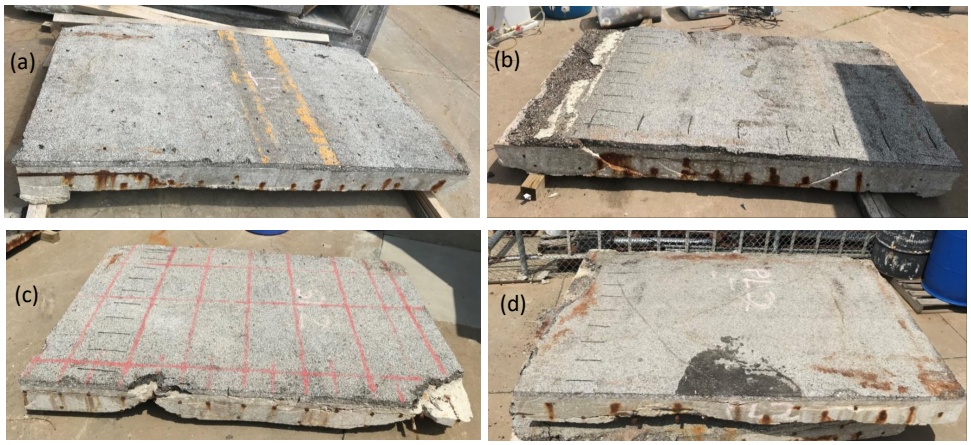

Fig. 2.11. Specimens from the Big Nehama river bridge bridge (a) MT1 (b) SL1 (c) SL2 (d) PL2

Concrete cover protects steel from corrosion, and a minimum cover thickness is required in reinforced concrete structures. For bridge decks, the cover depth can be determined when the velocity and TWTT are known. The previous sections have shown the procedures to measured TWTT between the deck surface and rebars, and to calculate the velocity in concrete cover in the sections 2.2 and 2.4. In order to demonstrate the accuracy of the depth calculations, the results need to be compared and verified with ground truth data.

At the beginning of the project, five bridge deck specimens with asphalt overlay were cut from a demolished bridge in Nebraska State Rte 105 over the Big Nehama River, Humboldt, NE. The specimens were named MT1, ML1, PL2, SL1, and SL2 according to their position on the bridge (mid-span, over pier (negative moment), inside and outside of travel lane). Figure 2.10 shows the location of each sample on the old bridge. Figure 2.11 shows the specimens stored at in the UNL structure laboratory area. Since ML2 was in severely deteriorated condition, it is not used in experiments. The results of the laboratory study on all four specimens are similar, therefore only the sample SL2 was used to present the result of GPR survey. Since the dimension of the specimens is relatively small compared to bridge deck, no deterioration maps are presented in this section.

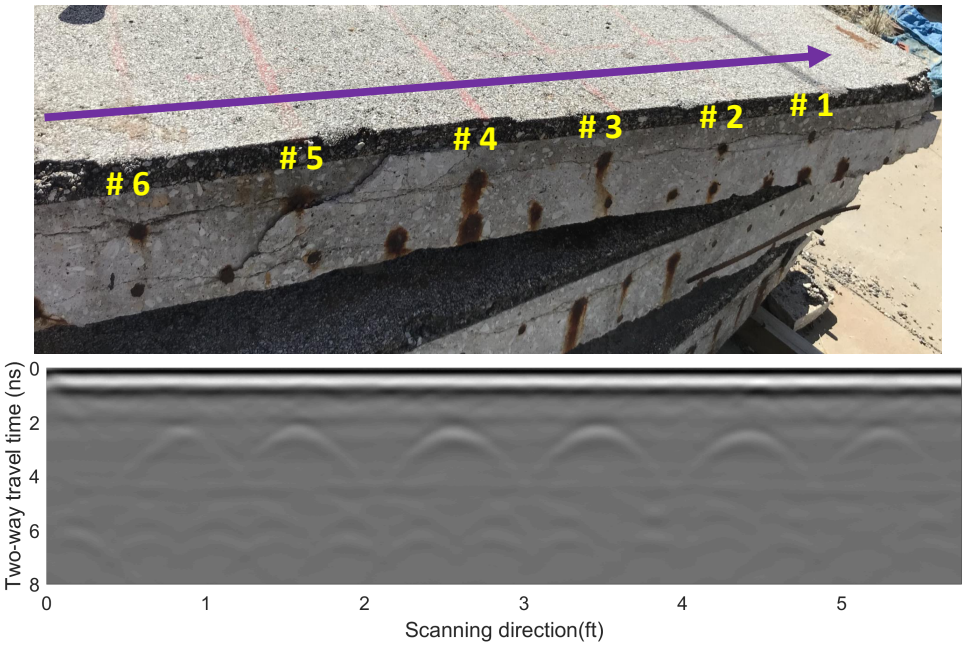

Fig. 2.12. GPR B-scan on the specimen SL2

Figure 2.12 shows one GPR B-scan on the SL2 specimen close to the edge from left to right. In Figure 2.12(a) the direction of scanning is shown as the arrow on the specimen. Six

exposed rebars from the top layer mat, are numbered and the result of the data processing is shown in Table 2.1. It is seen that the calculated rebar depths based on the wave velocity and TWTT calculation are close to the actual depths, with most errors within 0.3 in. Wave velocity around rebars #3 and #4 have strong reflection amplitudes and high velocity. This result is also expected, because lower wave velocity is a precursor parameter for deterioration. Average permittivity can be calculated from the velocity information, and also shown in the table, where ϵ_r is the average permittivity of concrete cover and asphalt overlay. The direct wave amplitude (surface amplitude) of the B-scan does not show significant variation, therefore, no information is obtained for the asphalt surface, which agrees with the clear surface condition shown in the picture. On the edge of the specimen, the horizontal crack (delamination) and rebar corrosion indicate severe deterioration in the concrete deck, which is not visible from the asphalt surfce. The large delamination width around rebars #6 and #1 may contribute to the low amplitude of GPR signals from these rebars.

Table 2.1. Summary of the GPR data processing on the specimen SL

Rebar number	Rebar depth measured (in)	Rebar depth GPR (in)	GPR velocity (in/ns)	ϵ_r cover	Surface Amp. (dB)	Rebar Amp. (dB)
1	3.4	3.1	3.89	9.2	-7.65	-11.88
2	3.5	3.3	3.94	9	-8.02	-5.33
3	3.2	3.1	4.23	7.8	-8.03	-3.7
4	3.3	3.2	4.15	8.1	-8.28	-2.95
5	3.3	3	3.98	8.8	-8.52	-6.88
6	3.1	2.6	3.7	10.2	-8.29	-13.518

2.9 Positioning and imaging

The GPR scanning cart is equipped with an encoder wheel, which is capable of measuring distance along the moving direction. Assuming that the GPR cart travels along a straight line, and by combining multiple parallel GPR scans a 2D image can be generated based on GPR signal analysis. More accurate positioning can be obtained using a Real Time Kinematic (RTK) GPS system for real time positioning. A U-blox RTK application board package (C94-M8P-2) was used in the field testing. That includes two RTK GNSS modules,

with one unit as the base and the other one as the rover. The base unit was installed at a corner of the bridge deck edge (reference point), and the rover unit was installed on the scanning cart. A coordinate system is built using the GPS base as the origin, the east direction as the X-axis, the north direction as the Y-axis, and the upward direction along the ellipsoid normal as the Z-axis. The relative position between the GPS rover and the base is defined as the scanning cart coordinate (x, y, z). The coordinates of the GPS rover were recorded continuously at a rate of one per second (1 Hz). Since it is convenient to show the scanning results using a local coordinate system, the GPS global coordinate system is converted to the local coordinate system, with the longitudinal direction of a bridge deck denoted as the X'-axis and the transverse direction of the deck as the Y'-axis. The Z'-axis is the same with the global coordinate system.

For every GPR B-scan a separate GPS file is recorded during the survey. The GPR B-scan path can be mapped using the GPS record. Therefore rebar locations on the bridge deck can be determined. These locations are scattered over the bridge deck with no regular pattern. A MATLAB function, *griddata*, use linear interpolation of amplitudes/velocity values in horizontal and lateral direction to map the GPR data on the rebar locations.

2.10 Summary of GPR data processing algorithm

The algorithm of the GPR processing is summarized in the Figure 2.13. Raw GPR data are first transferred to a computer, and then a MTALAB package developed by the research team is used for further processing. The procedure can be briefly described as follows:

1. Extract and store direct coupling wave amplitude;
2. Obtain zero-time for GPR reflection at the deck surface by subtracting the direct air wave from all signals, and shift the B-scan to correct zero time;
3. Reduce the clutter to increase contrast and visibility of the hyperbolas in the B-scan image;
4. Identify rebar positions using automated rebar picking algorithm;
5. Calculate the electromagnetic wave velocity in the cover depth above each rebar using the migration and statistics;
6. Extract migrated amplitude at each rebar location;
7. Calculate rebar depth using the TWTT and velocity for all rebars;
8. Normalize rebar reflection amplitude by the surface condition; and
9. Correct the amplitude with rebar depth.

The following maps can be generated from this analysis: direct coupling wave ampli-

tude on deck surface, wave velocity in concrete cover, cover depth, and GPR amplitude (attenuation). These maps will identify areas in the bridge deck with surface anomalies, concrete deterioration, cover thickness variation, or rebar corrosion. Further data analysis by combining or fusing the information will provide a comprehensive evaluation of the bridge deck.

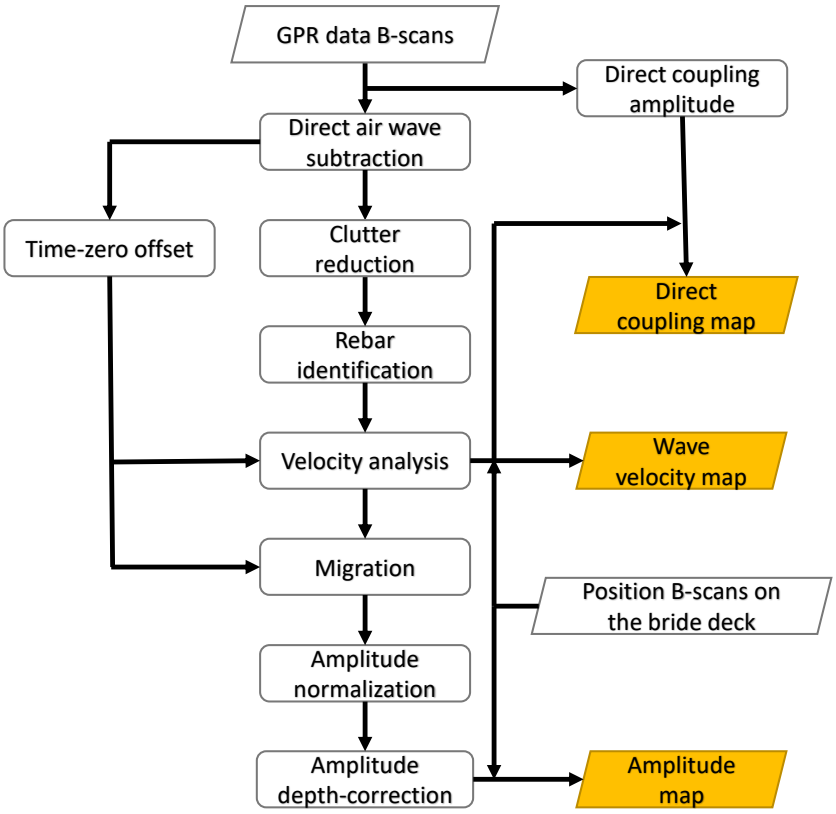

Fig. 2.13. The workflow of the GPR data processing

Chapter 3

GPR survey on bridges in Nebraska

The previous chapter presents the detailed GPR data processing procedures and addresses common issues in the current GPR practice. In this section, the developed analysis procedures are applied to GPR data collected from three bridges in the state of Nebraska, and results from the proposed data processing are presented and discussed.

3.1 Bridge ID: SL55W00049L

Fig. 3.1. Google map image of the bridge SL55W00049L (map data ©2018 Google)

The bridge SL55W00049L is a two-lane concrete bridge located in Lincoln, NE. The concrete bridge deck is 305.1 ft long and shown in the Figure 3.1. The bridge deck was tested in Summer of 2017. A GSSI SIR-3000 GPR system with a 1.5 GHz ground-coupled antenna unit was deployed for GPR survey. Because of time constraint during the field test, the line spacing between scans was set to 2 ft. Positions were recorded using the RTK GPS

unit which was discussed in the section 2.9.

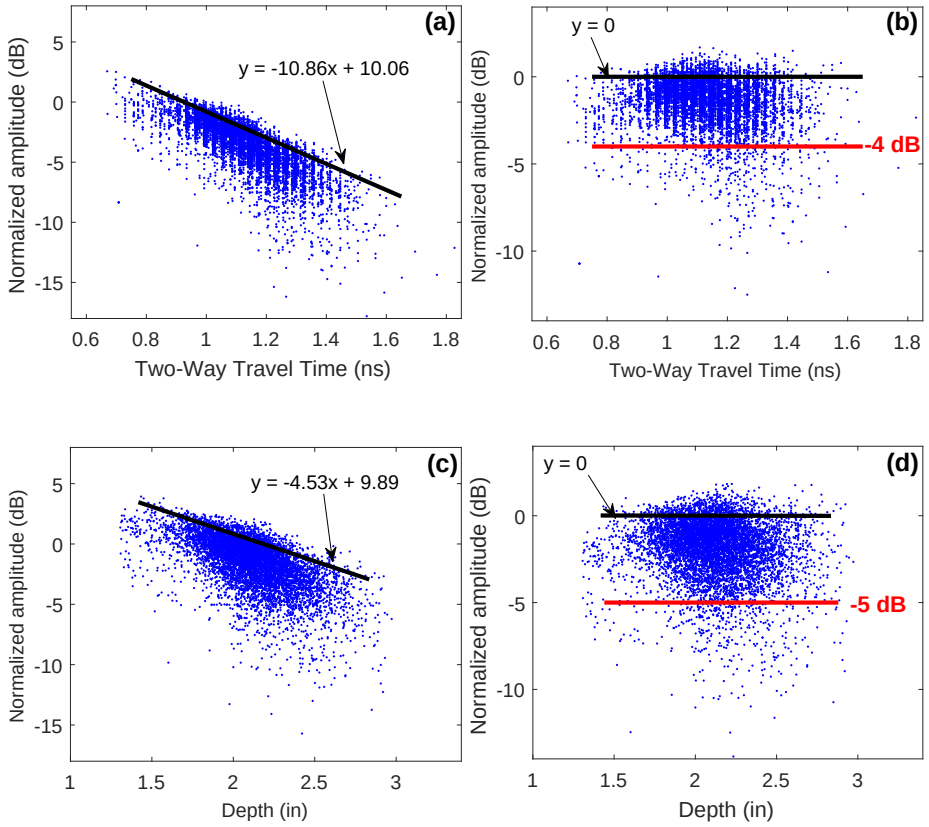

Fig. 3.2. GPR amplitudes. (a)-(b) normalized by a constant number and corrected with TWTT, and (c)-(d) normalized for each rebar and corrected with the rebar depth.

Figure 3.2 presents the scatter plots of GPR amplitude corrected by TWTT (a&b) and rebar depth (c&d) methods. Figure (a) and (b) represent the conventional analysis method, where the amplitudes were normalized by the maximum amplitude of the direct coupling wave from all scans on this bridge, which is a constant number for this specific bridge. In Figure (c) and (d), each data point was normalized by the amplitude of the direct coupling wave directly above the rebar, which varies for each rebar.

It can be seen that the data points have less scattering along the depth axis than the TWTT axis, which means the variation of actual rebar depth is less than that indicated by the TWTT. The 10 percentile fitting line has a larger amplitude range (steeper slope) in the TWTT plot (Figure (a)) than that in the rebar depth plot (Figure (c)), which means the data points tend to be over-corrected by the TWTT correction method. After depth correction, it is found that majority data points have an amplitude above -5 dB (Figure 3.2(d)). Therefore

the threshold value for amplitude is set at -5 dB for depth corrected amplitude. In a similar way, the threshold value for TWTT corrected amplitude is set at -4 dB.

With the GPR data processing procedures presented in the previous chapter, five images are generated. Figure 3.3(a) shows the rebar amplitudes normalized by a constant number and corrected with TWTT (conventional method). Figure 3.3(b) shows the rebar amplitudes using the new normalization method (varying direct-coupling amplitude) and corrected by the rebar depth. Gray color indicates sound concrete (low conductivity) and areas with low moisture content (low permittivity). These two images show areas of deterioration in almost the same locations. Most deterioration areas occur along two joints and in the mid-span. Low amplitudes may be caused by either corroded rebars, high conductivity in concrete, or combination of both effects. According to [23], concentration of ions in the concrete will increase both the dielectric permittivity and attenuation. Accumulation of deicing salt and moisture may induce low velocity and high attenuation. In previous analysis, we realized that the amplitude correction method by TWTT tends to over correct low amplitude data points with large TWTT, which leads to underestimation of deterioration in low velocity areas. For example, the map with TWTT correction shows less severity along the joints than the map with depth correction, because the joints have very low velocity (Figure 3.5(a)). In addition to using different depth correction methods, Figure 3.3(a) includes attenuation due to surface effects, but Figure 3.3(b) eliminates the effect of surface condition and only evaluates the soundness of cover concrete and reinforcements. Table 3.1 lists the deterioration area and percentage of the bridge deck for these two images. For this bridge, the difference between these two methods is very small.

Table 3.1. Summary of the GPR data processing on bridge SL55W00049L

	Old method	Proposed method
Area ft^2	394.5	404
Percentage %	3.2	3.3

Figure 3.4 shows the direct coupling wave amplitude map. Except for a few localized spots in the middle of the deck and at the end joints, the direct-coupling amplitude is low, which indicates that the concrete surface is generally in good and dry condition. As discussed earlier in the section 2.2, the direct coupling wave amplitude is sensitive to dielectric constant of the surface concrete, and low amplitude may indicate surface anomalies. Therefore, areas of concrete deck with low direct wave amplitudes are highlighted with red color

on the map. Comparing Figures 3.4 and 3.3(b) suggest that direct-coupling amplitude and rebar amplitudes are in general agreement in low amplitude regions.

Figure 3.5(a) is the wave velocity map over the entire bridge deck. Velocity is inversely related to permittivity of the concrete (see Eq. (1.1)). According to Klysz and Balayssac [24], relative permittivity of 7.5 approximately corresponds to concrete with saturation degree of 60%. Areas of high permittivity indicate existence of moisture. Rebars in highlighted areas are more likely to corrode than those in dry concrete shown with gray color. The velocity map in Figure 3.5(a) may indicate precursor of concrete deterioration which is represented by high permeability and high moisture contents. Figure 3.5(b) shows the calculated concrete cover thickness of the top layer reinforcements. Small cover thickness less than 2 inches are highlighted and dark red color indicates severe reduction of cover thickness (< 1.5 inch).

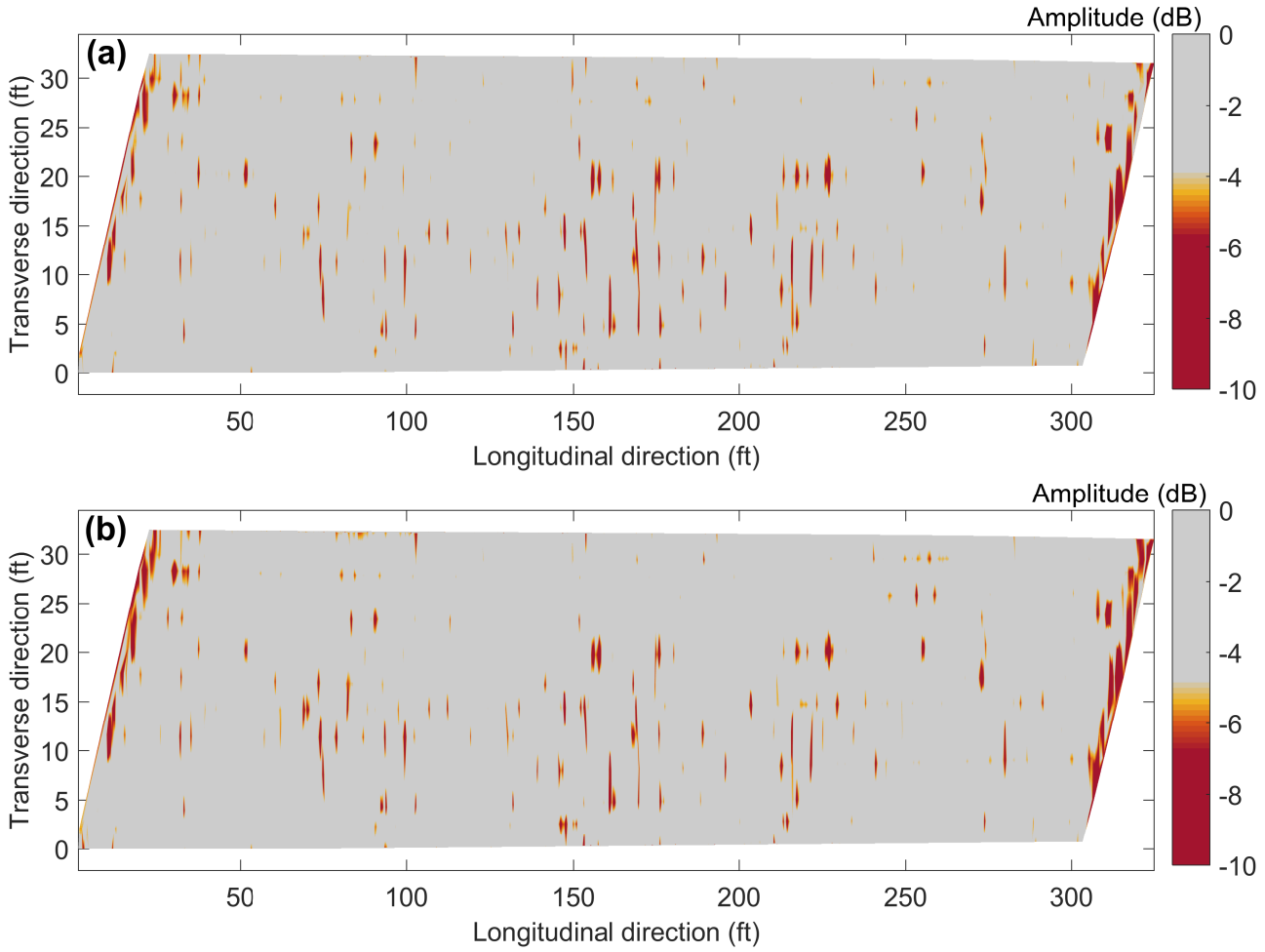

Fig. 3.3. Map of GPR amplitude normalized by the (a) a constant number and (b) proposed (varying from each rebar) methods.

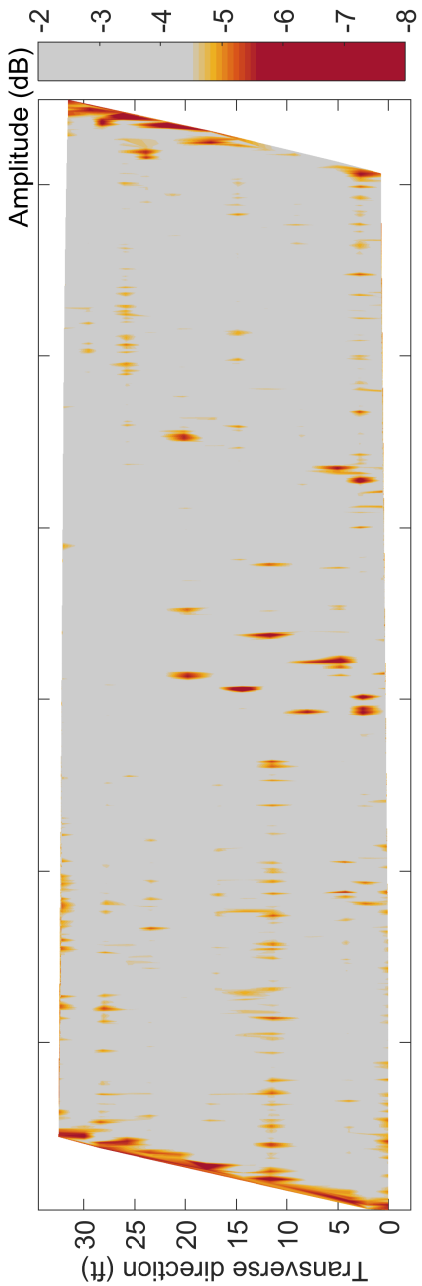

Fig. 3.4. Direct coupling amplitude map

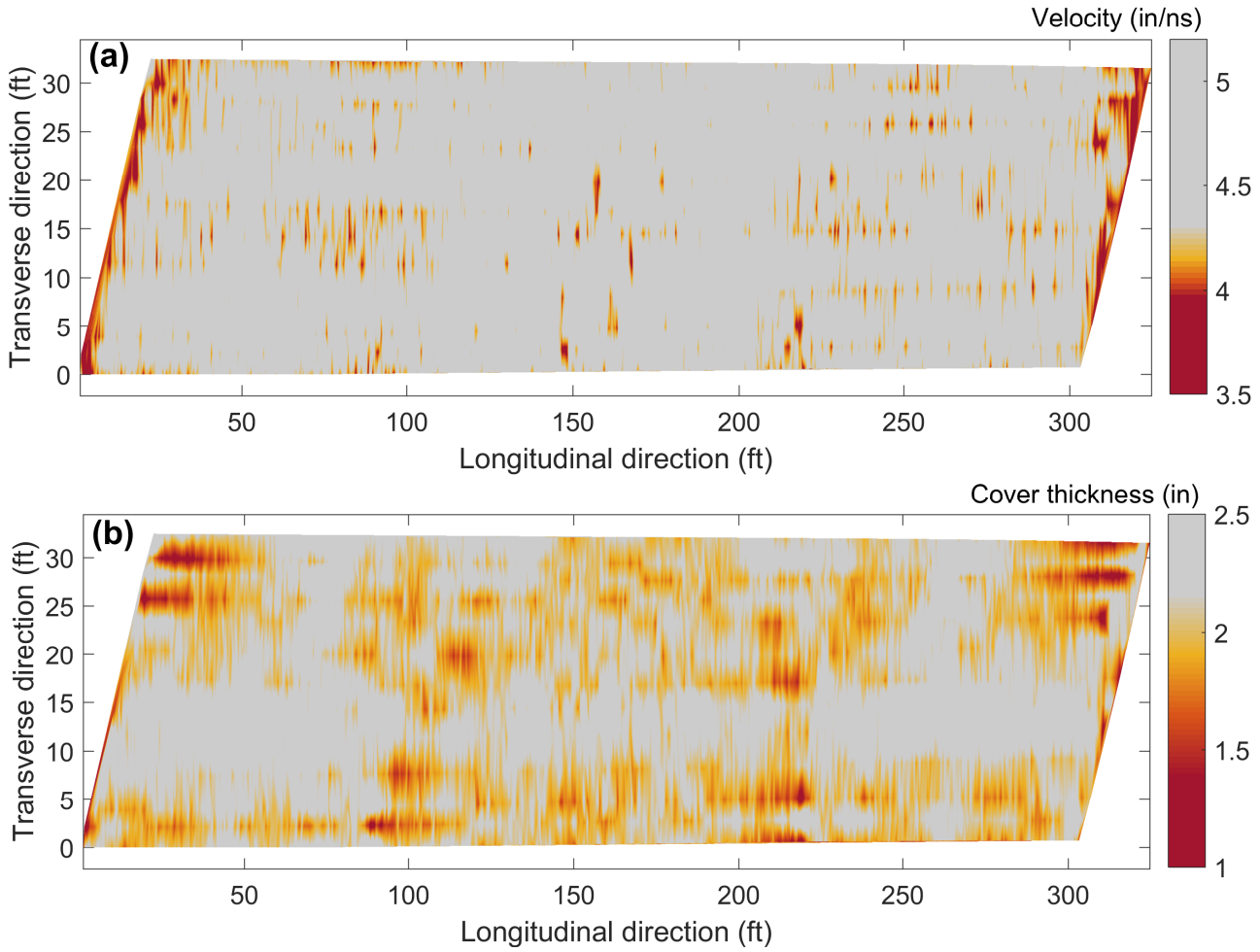

Fig. 3.5. (a) Velocity (b) cover thickness map

3.2 Bridge ID: C005512355

GPR survey on bridge C005512355 was conducted in Summer 2019 in Lincoln, Nebraska. The satellite image of the bridge is shown in the Figure 3.6. The asphalt overlaid bridge is 24 ft long and 28 ft wide that carries two-way traffic. A GSSI SIR-4000 GPR systems with 1.5 GHz antenna was used to test this bridge. The spacing between scan paths were 1 ft and 25 scans were recorded along the direction of traffic. For this short bridge, the positions of the reflections were calculated using GPR cart encoder.

Fig. 3.6. Google map picture of the bridge (map data ©2018 Google)

Figure 3.7 shows the scatter plots of the amplitude vs. TWTT (Figure (a)) and amplitude vs. rebar depth (Figure (c)), and the corrected amplitudes by TWTT (Figure (b)) and rebar depth (Figure (d)) respectively. The red lines represent the threshold amplitudes, which are the same as used in the analysis for bridge SL55W00049L. Compared to bridge SL55W00049L, this bridge is very short and there are not as many data points as in the former case. Therefore, the current depth correction analysis and threshold value might not be the most appropriate. We need to collect more data from bridge decks with asphalt overlays to improve the analyais accuracy.

Using the processing methods discussed earlier, five maps are generated based on the data. Figure 3.8 shows the rebars reflection amplitude map over the entire bridge. The amplitudes in Figure 3.8(a) were normalized by a constant number and then corrected by TWTT of the rebar reflections. The amplitudes in 3.8(b) were normalized by the direct coupling amplitude over each rebar and further corrected by calculated depth of rebars. The deteriorated area in both maps indicate that most of deterioration areas are along the traffic

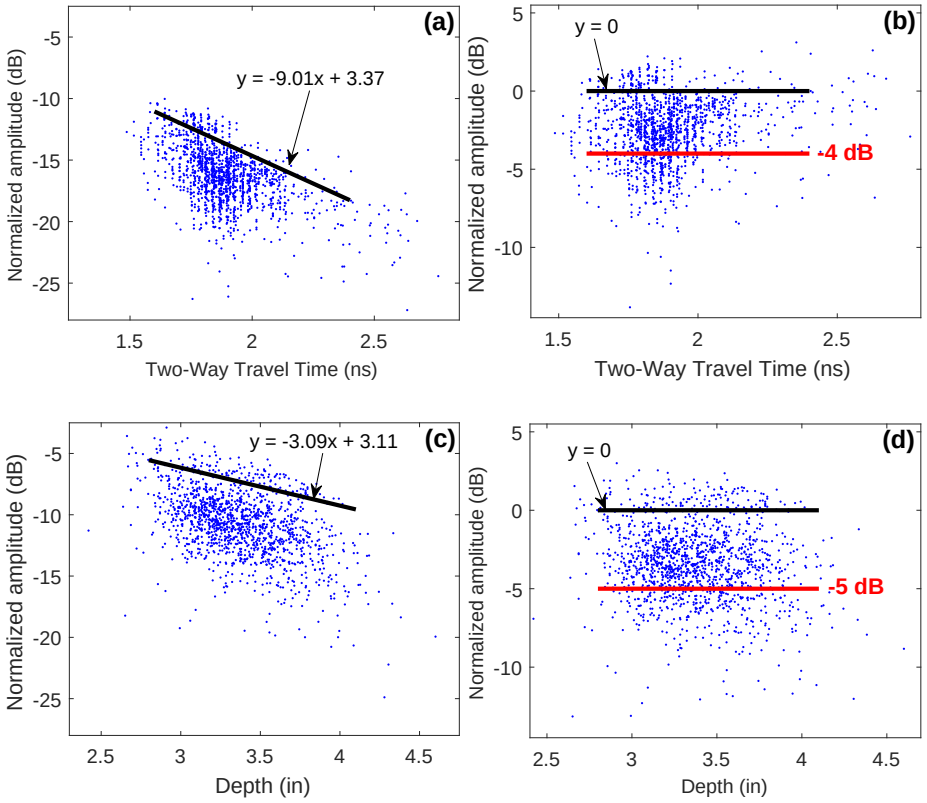

Fig. 3.7. Depth-correction of the amplitudes with (a)-(b) TWTT , and (c)-(d) depth

wheel paths in the middle of the bridge. However, high attenuation along the left joint only appear in the depth-corrected map (Figure 3.8(b)), not in the TWTT-correct map. Because the left joint has very low velocity, the rebar amplitudes were over-corrected when they were corrected by the TWTT method. Over-correction tend to happen in the low velocity regions.

In Table 3.2 the deterioration area on the bridge and its percentage are calculated for these two normalization and depth-correction methods. The proposed depth-correction method shows slightly more deterioration area than the old method. For this bridge, the difference between two methods is about 5 ft^2. Despite the slight difference, the old method missed the deteriorated area on the southern joint.

Figure 3.9 shows the amplitude map of the direct wave over the bridge. Since the bridge is asphalt covered, variation in amplitude indicates variation in bulk density of the asphalt material. In the highlighted areas, less energy could penetrated into the concrete than areas shown with gray.

Figure 3.10(a) shows the EM wave velocity map on the bridge. Areas with low velocity

Table 3.2. Summary of the GPR data processing on bridge C005512355

	Old method	Proposed method
Areaft^2	118	122.8
Percentage %	17.6	18.3

have high dielectric permittivity which may indicate moisture in concrete. Corrosion progresses faster in wet concrete than dry concrete. Therefore, these areas may have existing corrosion or are likely to corrode in the future. Figure 3.10(b) shows the cover thickness variation in concrete and asphalt. The numbers on colormap shows the sum of concrete and asphalt thickness over each rebar. The accuracy of the cover thickness calculation depends on the system resolution (here is a quarter of inch) and quality of the data.

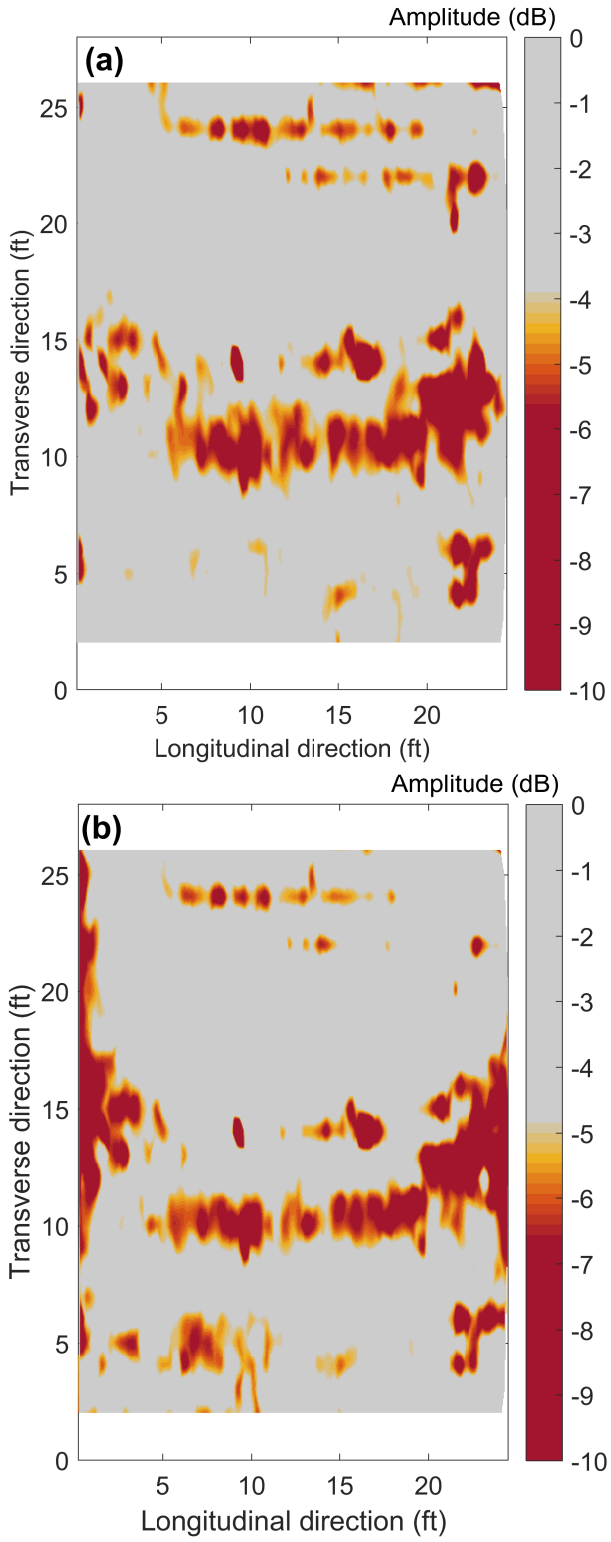

Fig. 3.8. Depth corrected rebar amplitude map with (a) normalization with constant number and depth-correction by TWTT (b) proposed normalization and depth-correction method

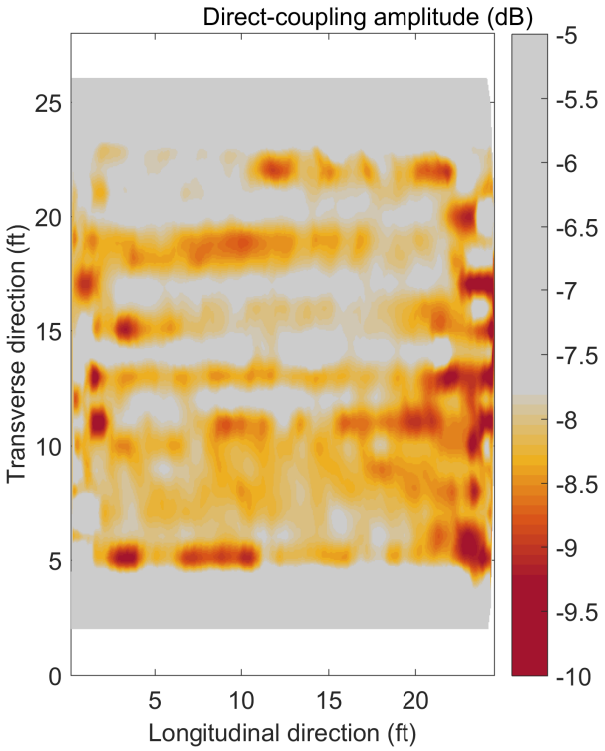

Fig. 3.9. Direct coupling amplitude map

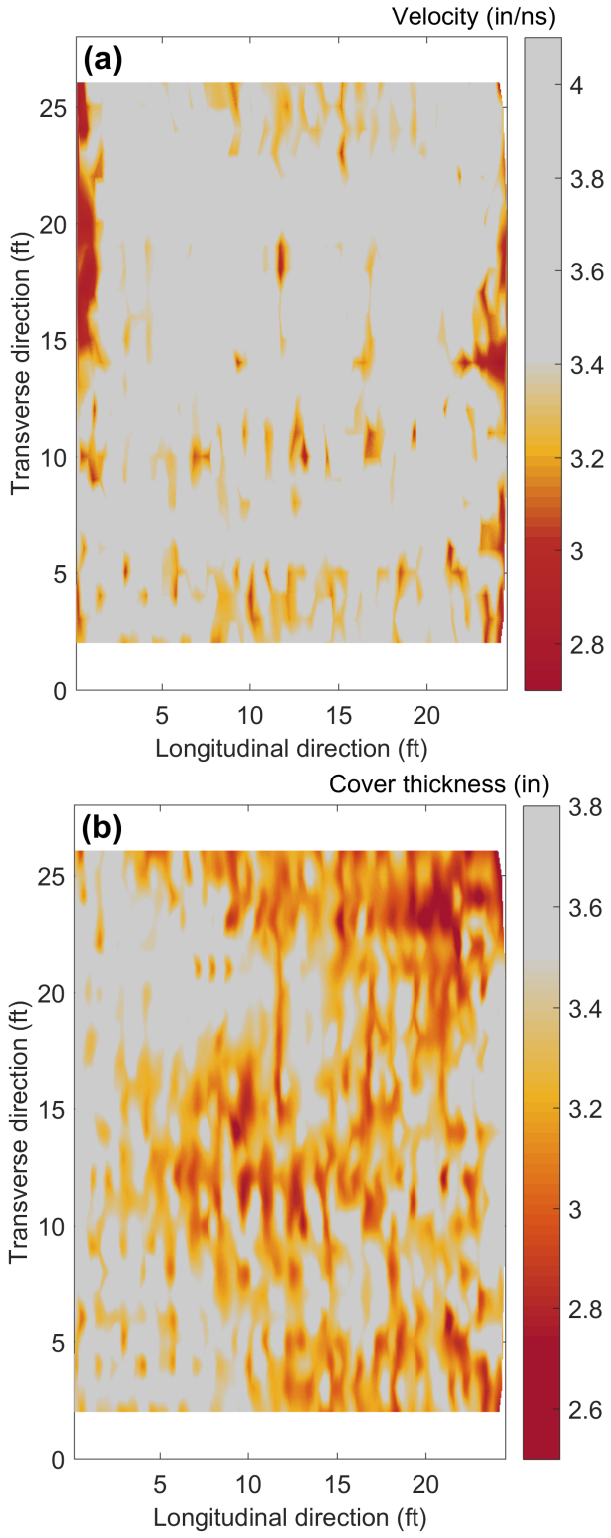

Fig. 3.10. (a) Velocity (b) concrete cover thickness maps

3.3 Bridge ID: S077 05693R

GPR survey on bridge S07705693R was conducted in Summer 2018 in Lincoln, Nebraska. The satellite image of the bridge is shown in the Figure 3.11. The concrete overlaid bridge is 180.1 ft long and carries one-way traffic. A GSSI SIR-4000 GPR systems with 1.5 GHz antenna was used to test one lane and one shoulder of this bridge due to time limitation and traffic control condition. The spacing between scan paths were 2 ft and 10 scans were recorded along the direction of traffic. For this bridge, the positions of the rebars were calculated using GPS device mounted on the suvey cart.

Fig. 3.11. Google map picture of the bridge S077 05693R (map data ©2018 Google)

Figure 3.12 shows the scatter plot of the amplitudes with and depth-correction procedure using TWTT and depth methods. Figure 3.12(b) shows the result of amplitude correction using TWTT data from Figure 3.12(a). After correction the red line indicates the threshold amplitude that separates the sound and the corroded rebars. This value is chosen based on the assumption that rebar amplitudes from sound rebars tend to form a condensed cluster of amplitudes [25]. Figure 3.12(d) shows the result of amplitude correction using rebar depth and the red line indicate the threshold amplitude of -5 dB. These threshold values are also supported by Dinh et al. [25].

Figures 3.13(a) and 3.13(b) show the amplitude of the bridge deck with the amplitude correction using TWTT and depth and the threshold value determined from the 3.12(b) and 3.12(d) respectively. With the new amplitude correction method, the deteriorated area of the bridge appears to be larger than in the image with TWTT amplitude correction. In both methods, the bridge deck joints show high attenuation which indicates high conductivity and chloride concentration. In the middle of the deck between 60 to 130 ft, the rebar depth corrected image shows a long strip of high attenuation area, which cannot be seen

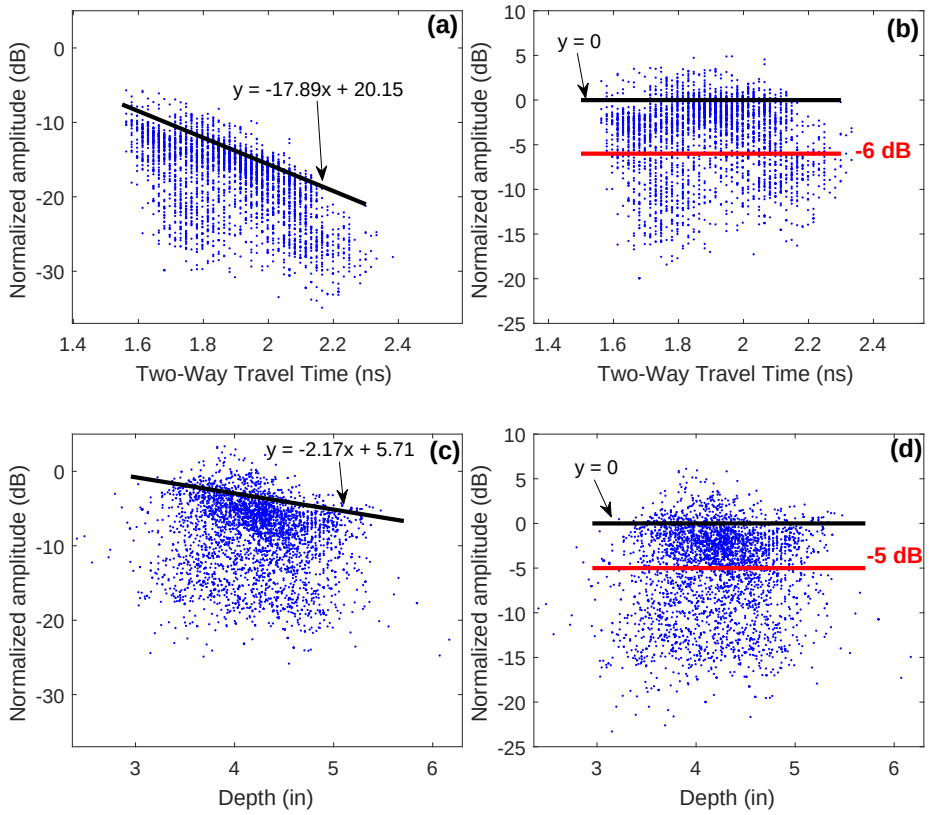

Fig. 3.12. Depth-correction of the amplitudes with (a)-(b) TWTT , and (c)-(d) depth

in the TWTT correct image (Figure 3.13(a)). When checking the direct coupling map in Figure 3.14 and velocity map in Figure 3.15(a), we notice the difference in amplitude maps correspond to regions with low direct coupling amplitude and low velocity.

Since the amplitude attenuates with distance, in bridges with large cover thickness (concrete + overlay) the difference between two amplitude correction methods becomes more pronounced in deteriorated regions, when compared to the bare concrete decks. In deteriorated areas where wave velocity is low, rebars appear in large TWTT's and thus, the rebar amplitudes will be over-corrected using the TWTT method. Table 3.3 shows highlighted area of the bridge deck in the Figure 3.13(a) and 3.13(b). As expected, the rebar depth correction method gives more deteriorated area than using the TWTT depth-correction method. In this bridge, the difference is quite significant with percentage difference about 15%.

Figure 3.14 shows the direct-coupling amplitude map of the bridge surface. In bridges with overlay, this amplitude indicate the condition of the overlay and do not provide any

Table 3.3. Summary of the GPR data processing on bridge S07705693R

	Old method	Proposed method
Area ft^2	1358	2342
Percentage %	20.3	35.1

information regarding the reinforced concrete bridge deck. If the deterioration in bridge deck is severe, its effect might appear in the direct-coupling map. In the Figure 3.14 highlighted areas with red color match the deterioration indicated by amplitude map (see Figure 3.13).

Figure 3.15(a) shows the wave velocity map over the bridge deck. Comparing the velocity map and the amplitude map (Figure 3.13(a)), we notice most highlighted low velocity regions are also included in the low amplitude map. With the velocity information and TWTT the cover concrete map is also plotted that gives the estimated rebar depth for this bridge (Figure 3.15(b)).

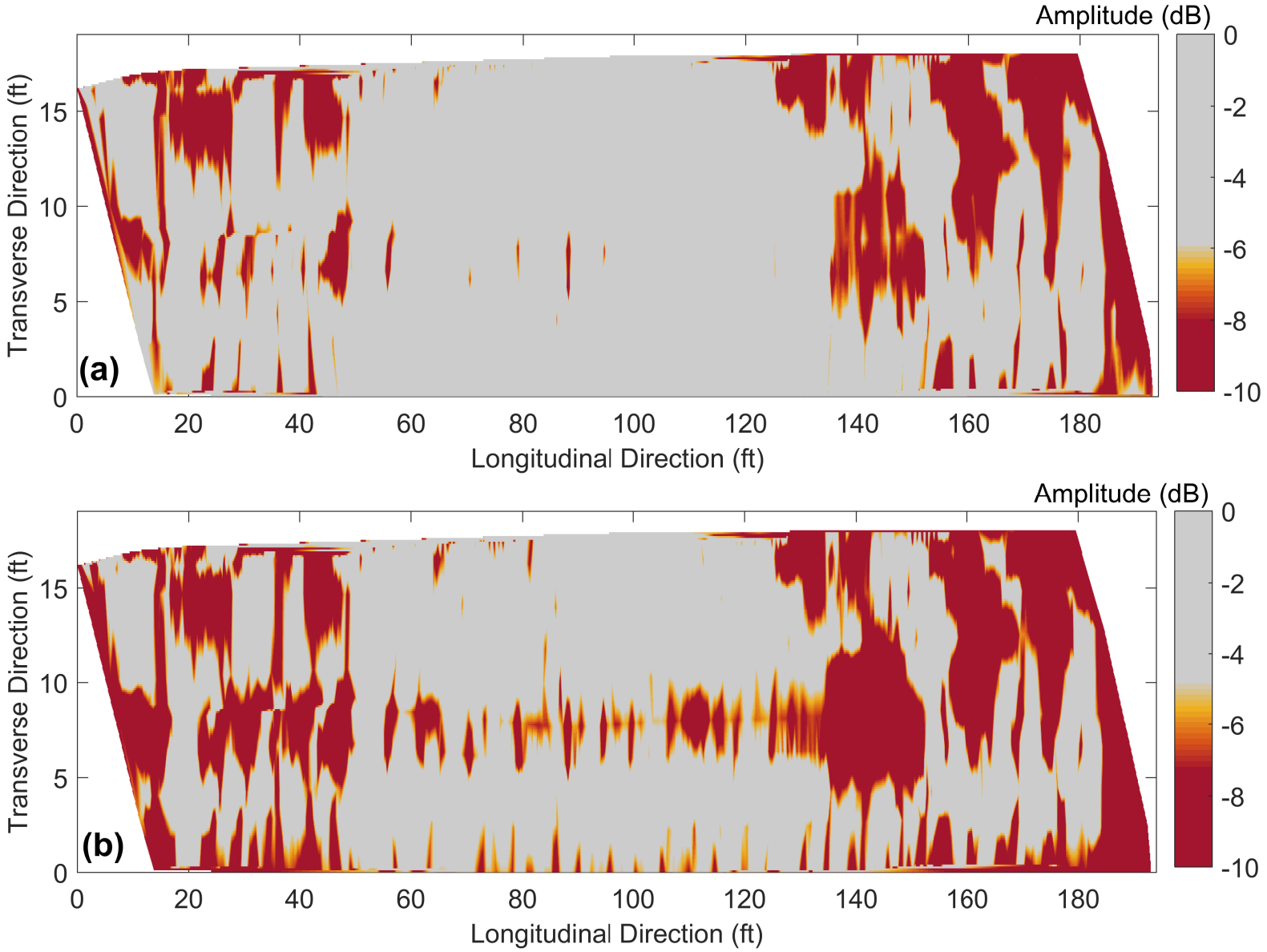

Fig. 3.13. Bridge S07705693R: Amplitude map generated with (a) the conventional method and (b) the proposed method (depth correction and surface normalization)

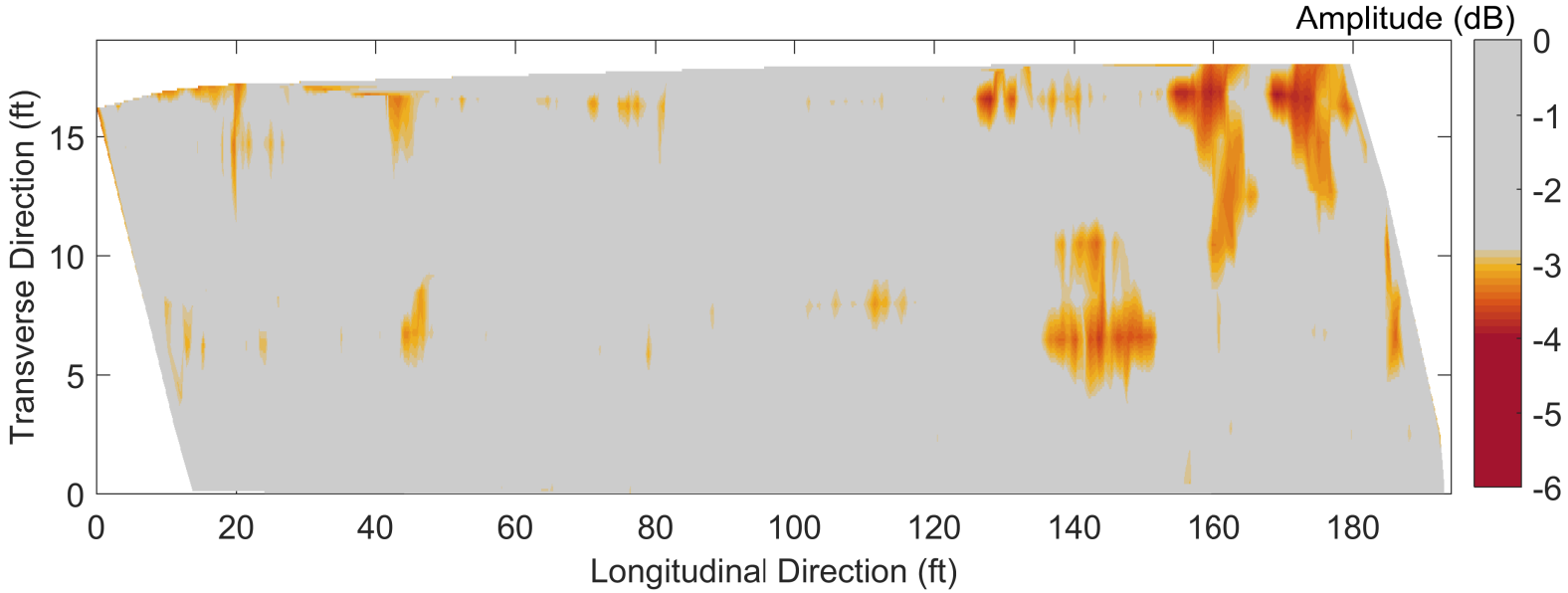

Fig. 3.14. Bridge S07705693R:Direct coupling amplitude map

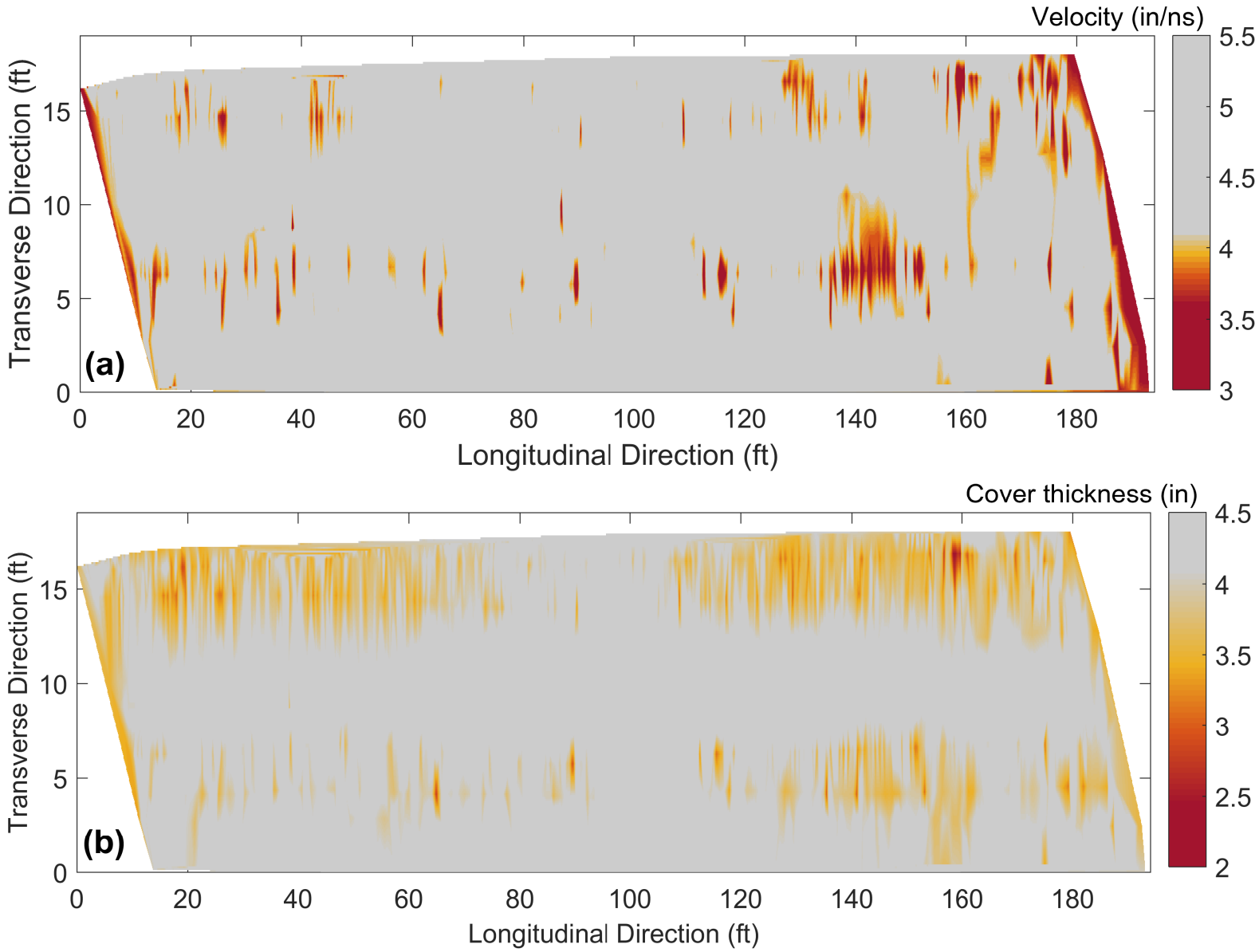

Fig. 3.15. Bridge S07705693R: (a) Velocity and (b) cover thickness maps

3.4 Discussion

The GPR data processing algorithm was implemented on three bridges with different types of overlays. The Proposed methods and processing steps worked well on all types of bridge decks. The most popular result from GPR data is the signal attenuation in the cover concrete of the top reinforcement mat. Increase of dielectric permittivity and conductivity in concrete cause attenuation of the signal. Therefore, excessive attenuation of energy in concrete gives alarms about the deterioration of concrete or rebar corrosion. By comparing the amplitudes of the reflected signals from rebars, we can evaluate the condition of steel and concrete . In attenuation maps shown in Figures 3.3(b), 3.8(b), 3.13(b), the signal attenuation is high at deck joints. In Nebraska during Winter, deicing salt is commonly used to melt ice/snow and keep roads safe after snowing/icing. Therefore chloride agents produced by deicing salt and water can seep into extension joints and provide a suitable environment for corrosion of steel reinforcements. In other parts of the bridge deck, chlorides can penetrate through cracks, reach rebars and remove the protective layer around steel rebars and start the corrosion

In bridge SL55W00049L, 3.3(a) and 3.3(b) do not show significant difference between different normalization methods and depth-correction procedures. However in bridges S07705693R and C005512355 (Figures 3.13 and 3.8), the proposed normalization and depth correction methods make a significant difference in final amplitude maps. The underlying reason of such difference is wave velocity in cover concrete and overlay. Rebars located in deteriorated regions show with low amplitude, high TWTT and large apparent depth. Thus these low amplitudes will be over-corrected when they are adjusted proportionate to TWTT, which will underestimate the low amplitude areas. Amplitude correction with actual rebar depths avoid these limitations, which allows comparing all rebar amplitudes at the same depth. Further research and experimental tests are needed in order to better explain the difference of GPR data processing on bridges with and without overlay and determine proper threshold values. In the 4.2 section, the future work plan is presented to better understand the results.

Chapter 4

Conclusions and future work

4.1 Conclusions

This report presents detailed GPR analysis procedures for condition assessment of concrete bridges. Compared to currently available data processing procedures, the presented work clarifies some common confusions and improves the efficiency of automated rebar picking algorithm. With the proposed procedure, we are able to generate four maps using parameters extracted from GPR signals.

Main conclusions are summarized as follows:

- For ground coupled GPR scans, relative permittivity of the concrete surface can be expressed by the direct wave amplitude. As relative permittivity increases, the direct wave amplitude decreases. The direct wave amplitude is correlated with internal condition of the concrete in severely deteriorated areas.
- With direct air wave subtraction, the surface reflection and rebar reflection have the same phase, which allows accurate calculation of the two way travel time and cover depth. The zero time can also be accurately determined from the break point of surface reflection. The result agrees with the method used by Yelf [17]. Accurate zero time is important for the migration algorithm.
- Velocity obtained by the permittivity of the concrete surface cannot accurately represent the velocity in cover concrete. Migration of GPR B-scans using the surface velocity gives inaccurate results. It may lead to over or under migration of the hyperbolas and inaccurate reflection amplitudes from rebars.
- Velocity in concrete can be obtained by using migration algorithm combined with a metric for migration performance. The velocity map might be used as precursor to

concrete deterioration.

- An automated rebar picking algorithm was developed to identify rebar reflections on migrated B-scan images. For bridge decks with regular rebar spacing, this algorithm is very efficient and effective. This method will be improved for GPR B-scans when rebars are heavily corroded or concrete is severely deteriorated.
- The proposed normalization method reduces the effect of surface conditions on the rebar reflection amplitudes. Deterioration can be categorized based on combined analysis of concrete surface reflection, velocity, and attenuation maps.
- The velocity information enables correction of rebar reflection amplitude with actual rebar depth, instead of using TWTT. On bridge decks with thick overlay, the traditional amplitude correction method with TWTT tends to over correct the low amplitudes and lead to underestimation of deterioration.
- The concrete cover thickness can be calculated using the the obtained velocity and TWTT. This cover thickness is an estimation actual cover thickness over reinforcements. The accuracy of the depth depends on the GPR system resolution.

4.2 Future work

Deterioration of concrete is a continuous process that starts when the structure's service life begins until the concrete component fails. Nondestructive testing of bridge decks can evaluate the deterioration condition of the structure at the time of survey, which is helpful in order to make timely repair decisions. Therefore, comparing the current NDT data to a reference point which corresponds to initial state of the concrete is necessary. In addition, change of NDT results over the life span of the concrete component accompanied by ground-truth data gives a very good estimation of the deterioration process in concrete.

Extracted parameters from GPR data such as rebar amplitude, wave velocity, and direct coupling amplitude provide information about the rebar corrosion process and deterioration of concrete. Once the value of these parameters reach a certain threshold, deterioration is in an alarming state when proper actions need to be taken. Therefore, the threshold value in GPR data analysis is the key to plot the deterioration map of the bridge deck instead of amplitude map, velocity map, etc.

Corrosion of reinforcements in concrete is one of the main reasons of concrete deterioration. Since GPR parameters are sensitive to rebar corrosion and moisture in concrete components, one way to determine the threshold value in GPR results is to induce corrosion in reinforced concrete and continuously monitor the progress of corrosion. By comparing

GPR data with other NDT results and ground-truth data, a threshold value can be determined. As the extention of this research project, we cast three reinforced concrete specimens with various cover thicknesses. These specimens will undergo biweekly wet and dry cycles with 5% salt-water solution until corrosion in reinforcements starts and further progresses over time. Within dry cycles many NDT data including, GPR, Half-Cell Potential, Resistivity, Ultrasonic, etc., will be collected on these specimens. by comparing multiple NDT data and statistical analysis, a threshold value for the GPR data will be established.

Bibliography

[1] R. Solimene, A. Cuccaro, A. Dell Aversano, I. Catapano, and F. Soldovieri, "Ground clutter removal in GPR surveys," *IEEE Journal of Selected Topics in Applied Earth Observations and Remote Sensing*, vol. 7, pp. 792–798, Mar. 2014.

[2] X. Wei and Y. Zhang, "Autofocusing techniques for GPR data from RC bridge decks," *IEEE Journal of Selected Topics in Applied Earth Observations and Remote Sensing*, vol. 7, pp. 4860–4868, Dec. 2014.

[3] C. Ozdemir, S. Demirci, E. Yigit, and B. Yilmaz, "A review on migration methods in B-Scan ground penetrating radar imaging," *Mathematical Problems in Engineering*, vol. 2014, pp. 1–16, 2014.

[4] K. Dinh, N. Gucunski, and T. H. Duong, "Migration-based automated rebar picking for condition assessment of concrete bridge decks with ground penetrating radar," *NDT & E International*, vol. 98, pp. 45 – 54, 2018.

[5] P. Kaur, K. J. Dana, F. A. Romero, and N. Gucunski, "Automated gpr rebar analysis for robotic bridge deck evaluation," *IEEE Transactions on Cybernetics*, vol. 46, no. 10, pp. 2265–2276, 2016.

[6] C. L. Barnes, J.-F. Trottier, and D. Forgeron, "Improved concrete bridge deck evaluation using GPR by accounting for signal depth-amplitude effects," *NDT & E International*, vol. 41, pp. 427–433, Sept. 2008.

[7] K. Dinh, N. Gucunski, J. Kim, and T. H. Duong, "Understanding depth-amplitude effects in assessment of GPR data from concrete bridge decks," *NDT & E International*, vol. 83, pp. 48 – 58, 2016.

[8] F. Xie, J. F.-C. Sham, W. W.-L. Lai, and X. Dérobert, "A modified algorithm for accurate gpr wave velocity estimation with common offset setting antenna," *2018 17th International Conference on Ground Penetrating Radar (GPR)*, pp. 1–6, 2018.

[9] W. L. Lai, T. Kind, and H. Wiggenhauser, "Detection of accelerated reinforcement corrosion in concrete by ground penetrating radar," in *Proceedings of the XIII Internarional Conference on Ground Penetrating Radar*, pp. 1–5, June 2010.

[10] A. Tarussov, M. Vandry, and A. De La Haza, "Condition assessment of concrete structures using a new analysis method: Ground-penetrating radar computer-assisted visual interpretation," *Construction and Building Materials*, vol. 38, pp. 1246–1254, Jan. 2013.

[11] GSSI, *RADAN 7 Manual*. Nashua, New Hampshire: Geophysical Survey Systems Inc., 2017.

[12] P. Kaur, K. J. Dana, F. A. Romero, and N. Gucunski, "Automated GPR rebar analysis for robotic bridge deck evaluation," *IEEE Transactions on Cybernetics*, vol. 46, pp. 2265–2276, 2016.

[13] K. Dinh, N. Gucunski, and T. H. Duong, "An algorithm for automatic localization and detection of rebars from GPR data of concrete bridge decks," *Automation in Construction*, vol. 89, pp. 292–298, 2018.

[14] C. Warren, A. Giannopoulos, and I. Giannakis, "Gprmax: Open source software to simulate electromagnetic wave propagation for ground penetrating radar," *Computer Physics Communications*, vol. 209, pp. 163 – 170, 2016.

[15] A. Di Matteo, E. Pettinelli, and E. Slob, "Early-time gpr signal attributes to estimate soil dielectric permittivity: A theoretical study," *IEEE Transactions on Geoscience and Remote Sensing*, vol. 51, pp. 1643–1654, March 2013.

[16] D. Comite, A. Galli, S. E. Lauro, E. Mattei, and E. Pettinelli, "Analysis of gpr early-time signal features for the evaluation of soil permittivity through numerical and experimental surveys," *IEEE Journal of Selected Topics in Applied Earth Observations and Remote Sensing*, vol. 9, pp. 178–187, Jan 2016.

[17] R. Yelf, "Where is true time zero?," in *Proceedings of the Tenth International Conference on Grounds Penetrating Radar, 2004. GPR 2004*, vol. 1, pp. 279–282, June 2004.

[18] K. Dinh, N. Gucunski, and T. Zayed, "Automated visualization of concrete bridge deck condition from GPR data," *NDT & E International*, vol. 102, pp. 120 – 128, 2019.

[19] W. Bi, Y. Zhao, C. An, and S. Hu, "Clutter elimination and random-noise denoising of GPR signals using an SVD method based on the Hankel matrix in the local frequency domain," *Sensors*, vol. 18, p. 3422, Oct. 2018.

[20] R. H. Stolt, "Migration by fourier transform," *Geophysics*, vol. 43, no. 1, pp. 23–48, 1978.

[21] F. Ahmad, M. G. Amin, and G. Mandapati, "Autofocusing of through-the-wall radar imagery under unknown wall characteristics," *IEEE Transactions on Image Processing*, vol. 16, pp. 1785–1795, July 2007.

[22] H. Sun, S. Pashoutani, and J. Zhu, "Nondestructive evaluation of concrete bridge decks with automated acoustic scanning system and ground penetrating radar," *Sensors*, vol. 18, no. 6, 2018.

[23] W. Lai, T. Kind, and H. Wiggenhauser, "Using ground penetrating radar and time-frequency analysis to characterize construction materials," *NDT & E International*, vol. 44, no. 1, pp. 111–120, 2011.

[24] G. Klysz and J.-P. Balayssac, "Determination of volumetric water content of concrete using ground-penetrating radar," *Cement and Concrete Research*, vol. 37, no. 8, pp. 1164–1171, 2007.

[25] K. Dinh, T. Zayed, S. Moufti, A. Shami, A. Jabri, M. Abouhamad, and T. Dawood, "Clustering-based threshold model for condition assessment of concrete bridge decks with ground-penetrating radar," *Transportation Research Record*, vol. 2522, no. 1, pp. 81–89, 2015.